Arrested coarsening of granular roll waves

D. Razis, A. N. Edwards, J. M. N. T. Gray, and Ko van der Weele

Citation: Physics of Fluids (1994-present) **26**, 123305 (2014); doi: 10.1063/1.4904520
View online: http://dx.doi.org/10.1063/1.4904520
View Table of Contents: http://scitation.aip.org/content/aip/journal/pof2/26/12?ver=pdfcov
Published by the AIP Publishing

Articles you may be interested in

Extreme waves induced by strong depth transitions: Fully nonlinear results
Phys. Fluids **26**, 051705 (2014); 10.1063/1.4880659

Linear and nonlinear stability of hydrothermal waves in planar liquid layers driven by thermocapillarity
Phys. Fluids **25**, 094101 (2013); 10.1063/1.4819884

Unconfined slumping of a granular mass on a slope
Phys. Fluids **25**, 023302 (2013); 10.1063/1.4792707

Decaying vortex and wave turbulence in rotating shallow water model, as follows from high-resolution direct numerical simulations
Phys. Fluids **24**, 115106 (2012); 10.1063/1.4767723

Density waves in gravity-driven granular flow through a channel
Phys. Fluids **14**, 3309 (2002); 10.1063/1.1499126

This article is copyrighted as indicated in the article. Reuse of AIP content is subject to the terms at: http://scitation.aip.org/termsconditions. Downloaded to IP: 150.140.170.210 On: Mon, 29 Dec 2014 14:07:55

CrossMark click for updates

Arrested coarsening of granular roll waves

D. Razis,[1,a)] A. N. Edwards,[2,b)] J. M. N. T. Gray,[2,c)] and Ko van der Weele[1,d)]
[1]*Department of Mathematics and Center for Research and Applications of Nonlinear Systems, University of Patras, 26500 Patras, Greece*
[2]*School of Mathematics and Manchester Centre for Nonlinear Dynamics, The University of Manchester, Manchester M13 9PL, United Kingdom*

(Received 23 June 2014; accepted 24 November 2014; published online 29 December 2014)

We study a system in which granular matter, flowing down an inclined chute with periodic boundary conditions, organizes itself in a train of roll waves of varying size. Since large waves travel faster than small ones, the waves merge, and their number gradually diminishes. This *coarsening process*, however, does not generally proceed to the ultimate one-wave state: Numerical simulations of the dynamical equations (being the granular analogue of the shallow water equations) reveal that the process is *arrested* at some intermediate stage. This is confirmed by a theoretical analysis, in which we show that the roll waves cannot grow beyond a certain limiting size (which is fully determined by the system parameters), meaning that on long chutes the material necessarily remains distributed over more waves. We determine the average lifetime τ_N of the successive N-wave states, from the initial state with typically $N = 50$ waves (depending on the length of the periodic domain) down to the final state consisting of only a handful of waves ($N = N_{\mathrm{arr}}$). At the latter value of N, the lifetime τ_N goes to infinity. At this point the roll waves all have become equal in size and are traveling with the same speed. Our theoretical predictions for the successive lifetimes τ_N and the value for N_{arr} show good agreement with the numerical observations. © *2014 AIP Publishing LLC.* [http://dx.doi.org/10.1063/1.4904520]

I. INTRODUCTION

When granular matter flows down an inclined channel as in Fig. 1, with a slope of about 35°, one may witness the spontaneous formation of so-called roll waves. These are traveling waves with sharp fronts, propagating at a speed exceeding the velocity of the grains themselves, separated by stretches of almost uniform thickness. Dramatic examples of this, often quite destructive, may be observed in debris flows, mud flows, and landslides around the world.[1] Indeed, granular roll waves are not only of intrinsic scientific interest but there is also an urgent practical need for understanding them better.

While roll waves in granular matter are a fairly new research theme,[2] similar waves in water and other traditional fluids have been studied for decades. Pioneering work was done by Cornish who, in two books published in 1910 and 1934, described roll waves in steep water channels, conduits, and spillways behind dams.[3,4] The free-surface instability responsible for the formation of the roll waves was revealed by Kapitza and Kapitza in 1949.[5] In the same year, Dressler published a mathematical study on roll waves that is still essential reading for anyone interested in the subject.[6–8] In the context of the present work, we also mention the paper by Chang *et al.* from 1996,[9] who realized that trains of roll waves in water undergo *coarsening*: since large waves move faster than small ones, they swallow the latter and thereby increase the typical distance between the waves. Finally, in 2004 Balmforth and Mandre[10] reported that this coarsening process—in a channel

a)Electronic mail: drazis@master.math.upatras.gr
b)Electronic mail: aedwards@maths.manchester.ac.uk
c)Electronic mail: nico.gray@manchester.ac.uk
d)Electronic mail: weele@math.upatras.gr

 ©2014 AIP Publishing LLC

This article is copyrighted as indicated in the article. Reuse of AIP content is subject to the terms at: http://scitation.aip.org/termsconditions. Downloaded to IP: 150.140.170.210 On: Mon, 29 Dec 2014 14:07:55

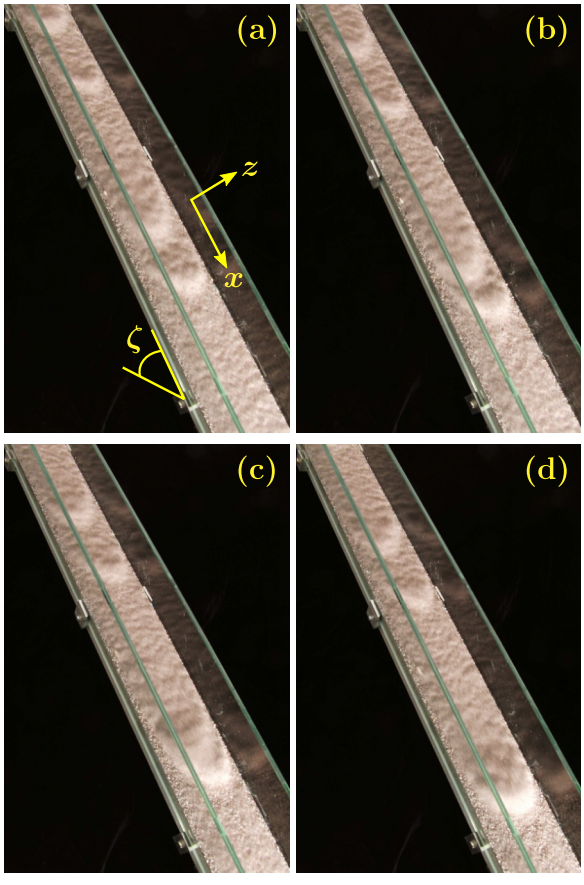

FIG. 1. Four photographs, 0.2 s apart, showing a section of about 50 cm of the experimental chute. In the first frame (a) we see four roll waves progressing down the chute. The leading wave is being overtaken by the second ((b)-(c)) and thereafter these two continue as one (d). The chute has a total length of 3.29 m, width 7.8 cm, and is inclined at an angle of $\zeta = 35.1°$ with the horizontal. The flowing grains are carborundum particles of 0.3-0.4 mm in diameter, with an average bed thickness of $h_0 = 4.2$ mm.

with periodic boundary conditions—does not necessarily continue all the way down to the 1-wave state, but may be interrupted at some intermediate stage with more than 1 wave. At this stage, the surviving waves have all become identical (and hence have equal velocities) and chase each other indefinitely.

The purpose of this paper is to describe the coarsening process of roll waves in dry granular matter, or sand, in a chute with periodic boundary conditions. Also in this case we will see that the coarsening is generally *arrested* before it arrives at the 1-wave state. We will show how this can be explained from the dynamical equations that govern the system.

In Sec. II, the governing equations of mass and momentum balance are introduced. They resemble the so-called shallow water equations for normal fluids, adapted where necessary to account for the special properties of granular matter, especially in the terms that represent friction and effective viscosity. Subsequently, in Sec. III, we present the results of a series of numerical experiments, starting out from a slightly perturbed sheet of flowing sand in a periodic chute of length L, and following its evolution (by numerically integrating the dynamical equations) in the course of time. It is here that we see that, if L is sufficiently long, the coarsening never reaches the 1-wave state. In Sec. IV, we describe the two opposing mechanisms that drive the coarsening process. The first mechanism is the *merging* of waves, caused by the fact that larger waves travel faster than small ones. The second mechanism is the *ripening* of waves: at each N-wave state, all the waves show a tendency to adapt their peak height to a given equilibrium value (and moreover, we show that there is an upper threshold this value can never exceed). Roll waves that are larger than

This article is copyrighted as indicated in the article. Reuse of AIP content is subject to the terms at: http://scitation.aip.org/termsconditions. Downloaded to IP: 150.140.170.210 On: Mon, 29 Dec 2014 14:07:55

this value spontaneously diminish their height (by shedding off mass) whereas smaller waves grow (by picking up some mass). The interplay between these two mechanisms controls the coarsening dynamics and determines at which stage it is arrested. In Sec. V, we develop a theoretical model for the coarsening process, which is based on these two opposing mechanisms. The paper culminates in a formula for the lifetime τ_N of the N-wave state. At the value $N = N_{\text{arr}}$, depending on the length of the chute and on the properties of the sand, this lifetime diverges. This is equivalent to saying that the coarsening process is arrested at the stage with N_{arr} waves. Finally, Sec. VI contains concluding remarks.

Before we turn to the analysis, let us briefly consider the system we are dealing with. We study a periodically extended version of the chute of Fig. 1. This means that the sand that leaves the system at the bottom of the chute re-enters the system at the top, instantaneously and without change of its profile or velocity. This allows the coarsening process (which takes a considerable time, especially during the final stages) to run its full course until it freezes in the state with N_{arr} waves. But of course the periodicity also introduces a connectedness between the downstream and upstream sections that a linear chute does not possess; so one should be cautious when translating our results to linear chutes, especially if the length L of the periodic domain is short. This is one of the reasons why we will focus mainly on long chutes.

Let us also mention the importance of the angle of inclination ζ. This should neither be too small (or the sand would simply sit still) nor too large (or the sand would be accelerated down the chute[11] until air drag and collisional stresses grow strong enough to balance gravity once again[12]). Only for angles between $\zeta_1 = 32.9°$ and $\zeta_2 = 42.0°$ there is a delicate, changing balance between the gravitational force that pushes the sand downwards and the friction from the floor of the chute that works in the opposite direction. In the setup of Fig. 1, the floor is roughened by means of spherical glass beads of 0.4 to 0.6 mm in diameter, which are glued to the chute, and the "sand" consists of carborundum particles of 0.3-0.4 mm in diameter. If we tilt the system at an angle of $\zeta = 35.1°$, a sheet of thickness $h_0 = 4.2$ mm (12 particle diameters) shows excellent spontaneous formation of roll waves and subsequent coarsening dynamics. Throughout the paper we assume that our system has the above well-balanced properties. A typical experimental run is presented in Fig. 2, where we see a train of roll waves and several merging events; the height of the waves (upper figure) is measured by means of a laser profilometer, while the space-time plot in the lower figure has been reconstructed from successive still images taken by a high-speed camera positioned above the chute.

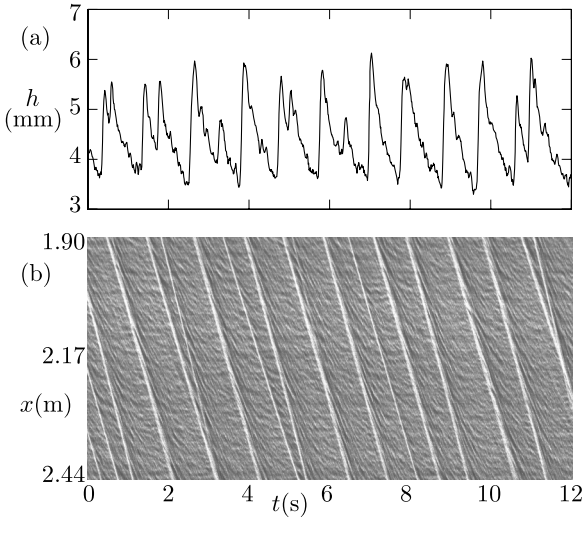

FIG. 2. Typical measurement of the flow thickness $h(x, t)$, at the position $x = 1.90$ m along the central axis of the chute, showing a train of roll waves passing by in the course of 12 s. Several pairs of waves are actually on the verge of merging. (b) The corresponding profile $h(x, t)$ between $x = 1.90$ m and 2.44 m, visualized by a high-speed camera during the same 12 s. The velocity of the wave crests (about 0.25 m/s) can be inferred from the slope of the contour lines. Wherever two lines are seen to meet, a merging event occurs.

This article is copyrighted as indicated in the article. Reuse of AIP content is subject to the terms at: http://scitation.aip.org/termsconditions. Downloaded to IP: 150.140.170.210 On: Mon, 29 Dec 2014 14:07:55

II. GOVERNING EQUATIONS

In order to study the behaviour of the moving granules, we use a hydrodynamic-like description, as for normal fluids, with properly modified friction and viscosity to take into account the special, granular nature of the flow. In this description, the two fundamental quantities to be determined are the height of the granular sheet, $h(x,t)$, and the depth-averaged velocity $\bar{u}(x,t)$

$$\bar{u}(x,t) = \frac{1}{h(x,t)} \int_0^{h(x,t)} u(x,z,t)dz, \tag{1}$$

where $u(x,z,t)$ is the velocity field of the grains in the chute (see Fig. 3). We ignore any variations in the crosswise (y) direction. The dynamical equations from which we determine the above two quantities are the continuity equation (expressing the conservation of material along the chute)

$$\frac{\partial h}{\partial t} + \frac{\partial (h\bar{u})}{\partial x} = 0, \tag{2}$$

and the depth-averaged momentum balance, which takes the following form:

$$\frac{\partial (h\bar{u})}{\partial t} + \frac{\partial (\chi h\bar{u}^2)}{\partial x} = hg\sin\zeta - \mu hg\cos\zeta - \frac{\partial}{\partial x}\left(\frac{1}{2}h^2 g\cos\zeta\right) + \frac{\partial}{\partial x}\left(\nu h^{3/2}\frac{\partial \bar{u}}{\partial x}\right), \tag{3}$$

which is reminiscent of the Savage-Hutter equation[13] but with an additional, novel viscous-like term[14] and a shape factor χ that is taken to be unity.

The continuity equation (2) simply states that a net influx of material into a fixed control volume, represented mathematically by $-\partial(h\bar{u})/\partial x$, gives rise to an increase in height $\partial h/\partial t$ in this control volume. Here, we assume that the granular material has a constant density ρ, i.e., that it may be treated as an incompressible fluid. This has also been used in the momentum balance, which has been divided by ρ throughout.

The momentum balance (3) expresses the fact that the change of momentum of the material contained in the control volume, given by the total (Stokesian) derivative on the left hand side, is equal to the resultant force on this volume. The contributing forces are [in the order in which they appear on the right hand side of Eq. (3)]

(i) The component of the gravitational force that acts along the chute, $hg\sin\zeta$ (with ζ being the angle of the chute with the horizontal);
(ii) the friction the granular material experiences from the bottom of the chute, $-\mu hg\cos\zeta$, which has the usual form of a friction coefficient μ times the normal force of the bottom acting on the granular material;

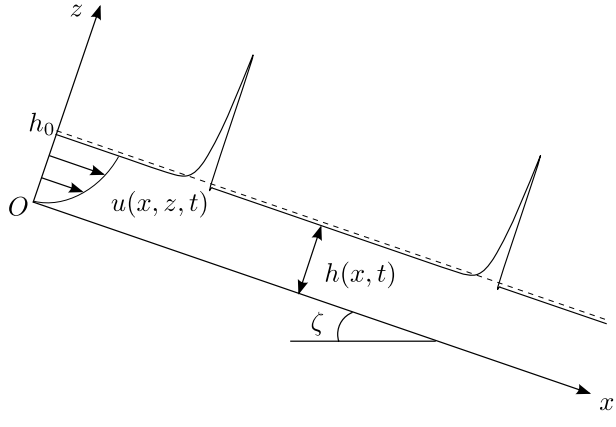

FIG. 3. Schematic diagram showing two roll waves propagating down a chute inclined at an angle ζ to the horizontal. There is a downstream velocity profile $u(x, z, t)$ (independent of the transverse coordinate y) and the dashed line at $z = h_0$ represents the uniform thickness of a steady, unperturbed flow.

This article is copyrighted as indicated in the article. Reuse of AIP content is subject to the terms at: http://scitation.aip.org/termsconditions. Downloaded to IP: 150.140.170.210 On: Mon, 29 Dec 2014 14:07:55

(iii) the depth-averaged pressure gradient $-\partial\left(\frac{1}{2}h^2 g\cos\zeta\right)/\partial x$ due to height variations of the granular sheet, assuming a standard hydrostatic (or rather lithostatic) pressure profile within the sheet;
(iv) the diffusive term $\partial/\partial x\left(\nu h^{3/2}\partial\bar{u}/\partial x\right)$, arising from depth-averaging the in-plane deviatoric stresses[14] assuming a $\mu(I)$-rheology[15] in the granular sheet.

Of the above terms, the friction and diffusion require some further discussion, since it is here that the granular nature of the medium is incorporated. With respect to the friction, we note that the coefficient μ in a flowing sheet of sand is not simply a constant (as in standard Coulomb friction) but has the rather more intricate form obtained by Pouliquen and Forterre[16]

$$\mu = \mu(h,\bar{u}) = \mu_1 + \frac{\mu_2 - \mu_1}{1 + \beta h^{3/2}\sqrt{g\cos\zeta}/(\mathcal{L}\bar{u})}. \tag{4}$$

This particular expression holds as long as the Froude number

$$\mathrm{Fr} = \frac{\bar{u}}{\sqrt{g\,h\cos\zeta}} \tag{5}$$

exceeds β, an empirical constant which for our chute is estimated to be $\beta = 0.65$. For Froude numbers below β, the friction is given by two alternative expressions,[16] one for the static case (Fr = 0) and the other for the intermediate regime $0 < \mathrm{Fr} < \beta$. All flows in the present paper, however, are such that the condition $\mathrm{Fr} > \beta$ is amply fulfilled (owing to the choice of the inclination angle ζ and the initial thickness of the sheet h_0) so the friction is always given by the dynamic friction law (4). The Froude number compares the depth-averaged velocity $\bar{u}$ with the velocity of gravity waves in a tilted sheet of fluid. Its value is related to the direction in which information is transferred through the sheet (in the inviscid case): for $\mathrm{Fr} > 1$, information can only propagate downstream, whereas for $\mathrm{Fr} < 1$ the information can propagate both upstream and downstream. In Eq. (4) for $\mu(h,\bar{u})$, the quantities

$$\mu_1 = \tan\zeta_1 \quad \text{and} \quad \mu_2 = \tan\zeta_2 \tag{6}$$

are the standard friction coefficients associated with the critical angles ζ_1 and ζ_2 discussed in the Introduction. The inclination ζ of our chute lies between these two values: $\zeta_1 < \zeta < \zeta_2$, since only in this regime do roll waves occur. The empirical constant $\mathcal{L} = 1$ mm is a characteristic length scale associated with a transition from ζ_1 to ζ_2 in the basal friction law.[16–18] In particular, the thickness of static material left on the chute, h_{stop}, by a steady uniform flow when the inflow is closed, is given by

$$h_{\mathrm{stop}}(\zeta) = \gamma\mathcal{L}, \quad \text{where } \gamma = \frac{\mu_2 - \mu_1}{\tan\zeta - \mu_1} - 1. \tag{7}$$

The definition of γ is a useful shorthand notation[19] that will be used later. For a steady uniform flow, with constant thickness and velocity, the only non-zero terms in Eq. (3) are those of gravity and friction (the first two terms on the right hand side), meaning that these must precisely balance each other, so $\mu = \tan\zeta$. Denoting the uniform thickness by h_0, the corresponding depth-averaged velocity is then found to be, through (4)

$$\bar{u}_0 = \frac{\beta\sqrt{g\cos\zeta}}{\mathcal{L}\gamma}h_0^{3/2} = Bh_0^{3/2}, \tag{8}$$

where for notational convenience we have introduced $B = \beta\sqrt{g\cos\zeta}\big/(\mathcal{L}\gamma)$. For the parameters used in the present paper, it has the value $B = 522\ (\mathrm{m}^{1/2}\,\mathrm{s})^{-1}$.

When the uniform flow thickness is reduced to h_{stop}, the Froude number (5) falls to the threshold value $\mathrm{Fr} = \beta$. In our system, to ensure that the Froude number remains above β everywhere and the material keeps flowing without exhibiting any stopping regions,[20] we take an initial thickness of $h_0 = 1.2h_{\mathrm{stop}}$.

To be specific, with $\zeta_1 = 32.9°$ ($\mu_1 = 0.647$), $\zeta_2 = 42.0°$ ($\mu_2 = 0.900$), and $\zeta = 35.1°$ ($\tan\zeta = 0.703$), we have $\gamma = 3.536$ and hence $h_{\mathrm{stop}} = \mathcal{L}\gamma = 3.536$ mm. So our choice $h_0 = 1.2h_{\mathrm{stop}}$ corresponds to a uniform thickness of 4.2 mm. As we will see in Sec. III (and as we have already seen

This article is copyrighted as indicated in the article. Reuse of AIP content is subject to the terms at: http://scitation.aip.org/termsconditions. Downloaded to IP: 150.140.170.210 On: Mon, 29 Dec 2014 14:07:55

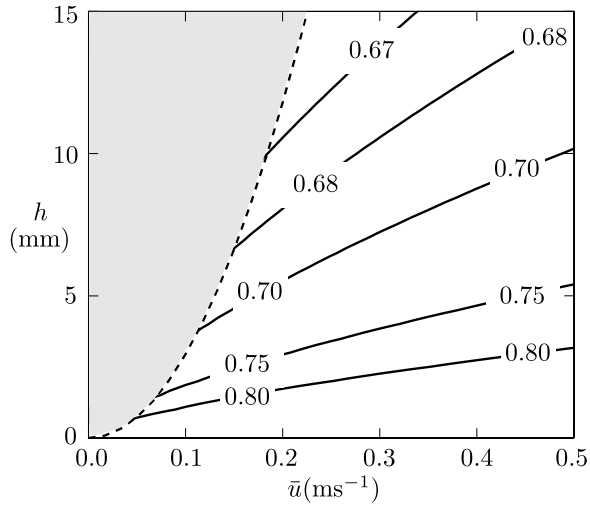

FIG. 4. Contour plot of the friction coefficient $\mu(h, \bar{u})$, given by Eq. (4), which is seen to decrease with growing flow thickness h and to increase with growing velocity $\bar{u}$. The shaded region corresponds to combinations of h and $\bar{u}$ when the granular layer is close to static (the corresponding Froude number is less than $\beta = 0.65$) and the given expression for μ does not apply. The dashed parabolic curve corresponds to the threshold $\mathrm{Fr} = \beta$.

in the experimental setup of the Introduction), the uniform flow under these conditions happens to be unstable: small random perturbations in the flow thickness do not damp out but tend to grow into well-developed roll waves.

Figure 4 illustrates how $\mu(h,\bar{u})$ depends on the local flow thickness $h(x,t)$ and the depth-averaged velocity $\bar{u}(x,t)$. It always remains close to the traditional Coulomb value $\tan\zeta = 0.703$, but the small variations around this value are of crucial importance. If $\mu(h,\bar{u})$ were constant, the material on the chute would simply accelerate indefinitely. By contrast, Fig. 4 shows that the friction force on the granular sheet is such that it slides more easily in regions where it is thick and flows slowly (large h, small $\bar{u}$), enabling small height perturbations of the uniformly flowing sheet to develop into roll waves.

We close with a few words on the diffusion term in Eq. (3). This term prevents the steep wave fronts from developing into discontinuous jumps, keeping the slope of the wave front to a finite (albeit large) value. It is derived from the $\mu(I)$-rheology for granular flow,[15] which is a nonlinear constitutive relation with a pressure and strain-rate dependent viscosity. To leading order this rheology implies that a steady uniform flow has a Bagnold velocity profile $u(z) \propto h^{3/2} - (h-z)^{3/2}$ and a lithostatic pressure $p(z) = \rho g(h-z)\cos\zeta$. To first order, depth-integration of the conservation equations for mass and momentum yields the shallow water-like equations (2)-(3), yet without the viscous term.[14] This set of equations has proved to be highly effective at modeling granular avalanches[13,21–23] and is capable of predicting the correct critical Froude number $\mathrm{Fr}_c = 2/3$ for the onset of roll waves,[24] though not yet the cut-off frequency.

A systematic extension to second order and higher is possible but complicated, generating a large number of additional terms that are difficult to interpret.[25] Gray and Edwards[14] therefore took a pragmatic approach and simply added the depth-averaged in-plane deviatoric stress to the momentum balance (3), i.e., the term

$$\frac{1}{\rho}\int_0^h \frac{\partial \tau_{xx}}{\partial x}\,dz = \frac{\partial}{\partial x}\left(\nu h^{3/2}\frac{\partial \bar{u}}{\partial x}\right). \tag{9}$$

Note that alternative forms of this viscous term are also possible, because the leading-order relationship between the depth-averaged velocity and the thickness ($\bar{u} \propto h^{3/2}$) can be used to reformulate it at this order. The version selected in (9) has been specifically chosen to ensure that the effective viscosity $(1/2)\nu h^{3/2}$ is non-singular for all inclination angles where roll waves appear $(\zeta_1 < \zeta < \zeta_2)$ and degenerates when $h = 0$, as it should.

This article is copyrighted as indicated in the article. Reuse of AIP content is subject to the terms at: http://scitation.aip.org/termsconditions. Downloaded to IP: 150.140.170.210 On: Mon, 29 Dec 2014 14:07:55

This approach is more powerful than one might expect, since Gray and Edwards[14] showed that the system (2)-(3), now including the viscous term, was able to quantitatively match the experimental cut-off frequency for roll waves[24] without any fitting parameters. In addition, Edwards and Gray[20] have shown that at low flow rates this viscous term plays a crucial role in the formation of erosion-deposition waves, which exhibit completely static regions ahead of and behind a solitary traveling wave.[26–29]

The coefficient ν in the viscous term (9) can be determined directly from the $\mu(I)$-rheology. It takes the form[14]

$$\nu = \frac{2\gamma\mathscr{L}\sqrt{g}\sin\zeta}{9\beta\sqrt{\cos\zeta}}, \tag{10}$$

which for the system under consideration means that $\nu = 2.4\ 10^{-3}\mathrm{m}^{3/2}\mathrm{s}^{-1}$. The value of this coefficient depends on the inclination angle: taking also into account the ζ-dependence of γ [Eq. (7)], it is seen that ν decreases with growing ζ, indicating that granular flows will experience a lower viscosity if the chute is made steeper. Here, one should keep in mind that our analysis is restricted to the range of angles where roll waves are encountered (i.e., $\zeta_1 < \zeta < \zeta_2$); also the aforementioned successful matching[14] of the experimental cut-off frequency for roll waves[24] lies of necessity within this range. We emphasize this because it is important to sound a note of caution that the present theory should not be taken beyond its bounds. For $\zeta < \zeta_1$ or $\zeta > \zeta_2$, the expression (10) yields negative values for ν and the theory becomes ill-posed,[14] echoing the underlying ill-posedness of the $\mu(I)$-rheology at low and high inertial numbers, respectively.

III. NUMERICAL OBSERVATIONS

The conservation equations (2)-(3) are numerically integrated using a solver based on the high-resolution non-oscillatory central scheme of Kurganov and Tadmor,[30] with the time evolution being carried out by a second-order Runge-Kutta method with a step size of 10^{-2} s.

The computational domain has periodic boundary conditions at the ends $x = 0$ and $x = L$, and the domain length L is discretized over 40 grid points per metre (i.e., 2000 grid points for a typical domain with $L = 50$ m) unless otherwise stated. The results have been checked for consistency on higher resolution grids. The higher resolution helps to smooth the artificial spikes in $h(x,t)$ that can be observed in front of the wave peaks for our standard resolution, while in all other respects the results are the same. In view of the fact that simulations on the finer grid require much longer computing times, we choose the standard resolution mentioned above in order to be able to do as many runs as possible (because we need good statistics) on a sizeable domain.

The initial conditions are those of a randomly perturbed steady uniform flow,

$$\begin{aligned} h(x,t=0) &= h_0 + \epsilon H(x), \\ m(x,t=0) &= m_0 = h_0\bar{u}_0, \end{aligned} \tag{11}$$

where $m(x,t)$ represents the volumetric flux (per unit width of the chute) of the granular material. The uniform flow velocity $\bar{u}_0$ is related to h_0 via the relation (8) and $\epsilon = 10^{-4}$ m (=0.1 mm) is the amplitude of the zero-mean perturbation $H(x)$, which picks a random value from the interval $[-1,1]$ at each grid point. The uniform flow thickness is set to $h_0 = 1.2h_{\mathrm{stop}} = 4.2$ mm in all simulations to ensure that the material keeps flowing continuously, with $\mathrm{Fr} > \beta$ everywhere; the expression (4) for the friction coefficient $\mu(h,\bar{u})$ then holds throughout.

The system of governing equations (2)-(3) is written in the vector form of convection-diffusion equations required by the numerical scheme, as follows:

$$\frac{\partial \boldsymbol{w}}{\partial t} + \frac{\partial \boldsymbol{f}(\boldsymbol{w})}{\partial x} = \boldsymbol{S}(\boldsymbol{w}) + \frac{\partial}{\partial x}\left(\boldsymbol{Q}(\boldsymbol{w},\boldsymbol{w}_x)\right), \tag{12}$$

This article is copyrighted as indicated in the article. Reuse of AIP content is subject to the terms at: http://scitation.aip.org/termsconditions. Downloaded to IP: 150.140.170.210 On: Mon, 29 Dec 2014 14:07:55

where $\boldsymbol{w} = (h, m)^{\mathrm{T}}$ is the vector of conserved variables h and $m = h\bar{u}$. The vectors for the convection flux $\boldsymbol{f}$, source term $\boldsymbol{S}$, and diffusive flux $\boldsymbol{Q}$ then take the form

$$\boldsymbol{f} = \begin{pmatrix} m \\ \dfrac{m^2}{h} + \dfrac{h^2}{2} g \cos\zeta \end{pmatrix},$$

$$\boldsymbol{S} = \begin{pmatrix} 0 \\ hg\left(\sin\zeta - \mu \dfrac{m}{|m|}\cos\zeta\right) \end{pmatrix},$$

$$\boldsymbol{Q} = \begin{pmatrix} 0 \\ \nu h^{1/2}\left(\dfrac{\partial m}{\partial x} - \dfrac{m}{h}\dfrac{\partial h}{\partial x}\right) \end{pmatrix}, \tag{13}$$

respectively, where the friction coefficient is given in terms of the conserved variables as

$$\mu = \mu(h, m) = \mu_1 + \frac{\mu_2 - \mu_1}{1 + \beta h^{5/2}\sqrt{g\cos\zeta}/(\mathcal{L}m)}\,. \tag{14}$$

In Fig. 5, we present the results of a sample simulation, carried out on a small domain of length $L = 3.20$ m, discretized over 3200 grid points, at several instants in time. Clearly, the upper plot (at $t = 116.0$ s) corresponds to an already advanced stage in the coarsening process. It shows two waves, A and B, which have originated from the coalescence of several smaller waves, which in turn emerged from the random initial conditions (11). The larger wave A travels with a greater speed than wave B, such that it catches up to B and merges with it, and from $t = 155.3$ s onward they are seen to form a single wave AB that is larger and faster than either of its composite parts. This is the basis of the coarsening behavior that is observed for larger wave trains on longer computational domains; the present example (Fig. 5) is only special insofar as the domain is sufficiently short to sustain a final 1-wave final state. That is, the coarsening in this case is not arrested in any intermediate multi-wave state but reaches its ultimate goal.

From the final two snapshots of Fig. 5, we also get a first glimpse of the second mechanism that will play an important role in our analysis of the coarsening process: The height of the wave AB does not maintain the exact value it has right after the merging event (which happens to be 8.25 mm) but in the course of time relaxes to the somewhat lower value of 7.98 mm. This we call the *equilibrium height* of the roll wave, which depends on the various system parameters and the dimensions of the chute, as we shall see later.

The results of a typical simulation on a domain of length $L = 50$ m are shown in Fig. 6 at seven successive moments in time. Here, the number of roll waves emerging from the perturbed uniform flow is approximately 80, which gradually decreases to a 6-wave state, at which point (for this particular run) the coarsening process is arrested; the six surviving waves are all seen to relax to the same equilibrium height 9.27 mm. The exact number of waves in the arrested state varies between the different simulations, owing to the randomness of the initial conditions. The coarsening process is most commonly arrested in a state with 6 or 7 waves. But arrested states with as many as 13 surviving states, or as few as 4, are also occasionally observed. The minimal value depends on the length of the chute: on the 50 m chute of Fig. 6, the coarsening process was never seen to get beyond the 4-wave states. On a similar chute with a periodic domain of $L = 25$ m (on which we also did extensive measurements), the corresponding minimal value was found to be 2 waves. The most commonly observed arrested state in this case consisted of 3 or 4 waves, and occasionally the coarsening process already came to a halt with as many as 10 waves.

In the context of coarsening, the key quantity of interest is the *average lifetime* τ_N of the successive N-wave states. Obviously, this lifetime grows during the course of the coarsening process, i.e., it should be a decreasing function of N. Figure 7 gives the measured values of τ_N versus N, collected from 100 simulation runs for periodic domains of length $L = 50$ m and $L = 25$ m.

This article is copyrighted as indicated in the article. Reuse of AIP content is subject to the terms at: http://scitation.aip.org/termsconditions. Downloaded to IP: 150.140.170.210 On: Mon, 29 Dec 2014 14:07:55

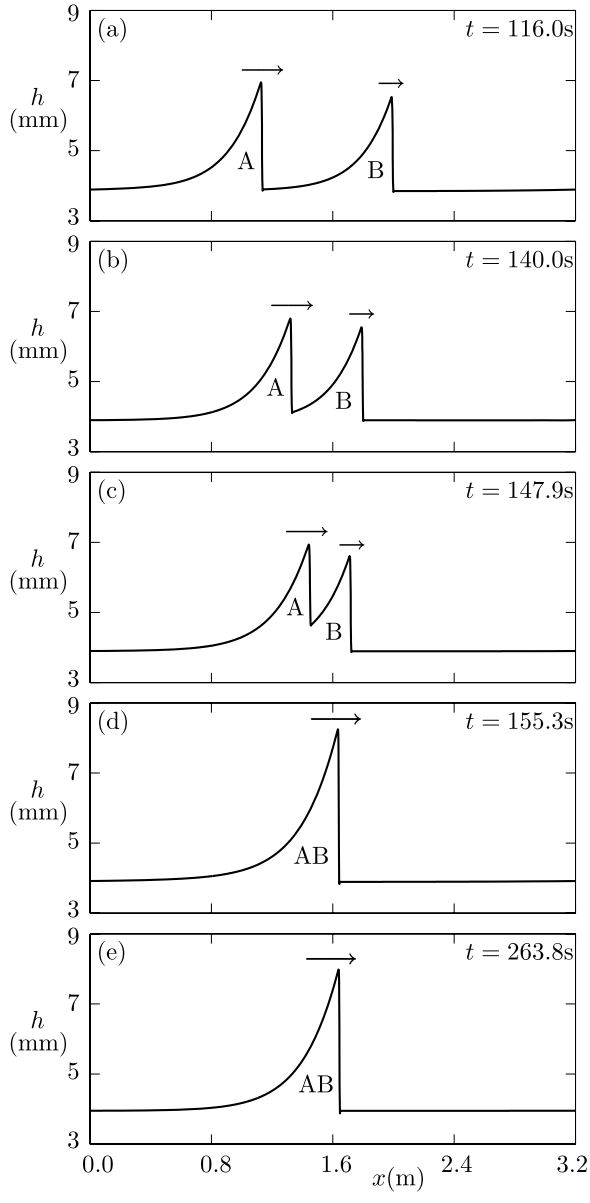

FIG. 5. Two roll waves A and B chasing each other in a chute of length 3.20 m with periodic boundary conditions. At $t = 155.3$ s, the larger (and therefore faster) wave A is seen to catch up with B and the two waves merge. From this moment on, A and B continue as one roll wave (AB) forever.

The τ_N are averaged over the number of runs in which each N-wave state is observed. Especially toward the end of the coarsening process, this number falls far below 100. Moreover, we exclude the arrested state of each run to avoid spurious divergences. (If one would include these states, τ_N would diverge for all values of N at which the coarsening is ever seen to be arrested; for the 50 m chute this would mean at all $N = 4,5,\ldots,13$.) The error bars in Fig. 7 represent the standard error of the measured data. Note that in both cases, the average lifetime is seen to rise steeply towards the end of the coarsening process (for small values of N) and that there are no measurements at all for $N \leq 4$ and $N \leq 2$, respectively, in accord with our earlier observation that the coarsening is never seen to proceed beyond these values.

In Sec. IV, we describe the mechanisms behind the coarsening process from which we subsequently derive a theoretical expression for τ_N.

This article is copyrighted as indicated in the article. Reuse of AIP content is subject to the terms at: http://scitation.aip.org/termsconditions. Downloaded to IP: 150.140.170.210 On: Mon, 29 Dec 2014 14:07:55

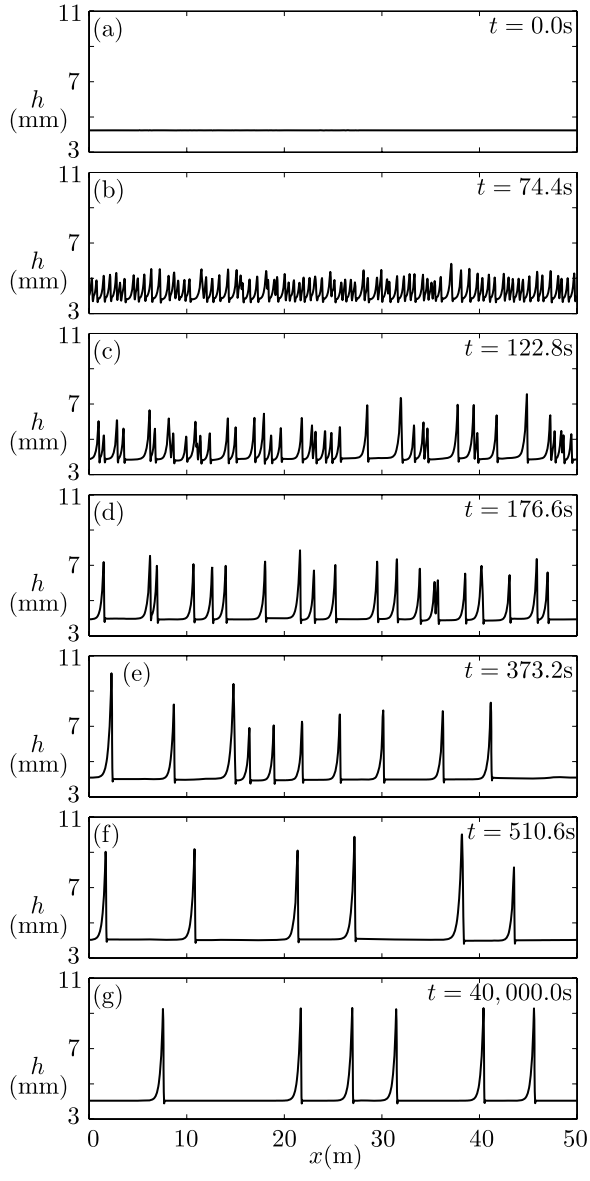

FIG. 6. Snapshots of a long time numerical simulation for a chute of 50 m length, with periodic boundary conditions, illustrating the sequence of merging events up to the final stage where the coarsening process is arrested. (a) $t = 0$ s: The initial stage corresponding to a random perturbation of the uniform flow (the amplitude of the perturbation is too small to be visible on this scale), (b) $t = 74.4$ s: approximately 80 peaks, not necessarily fully developed roll waves yet, (c) $t = 122.8$ s: 40 roll waves, (d) $t = 176.6$ s: 20 roll waves, (e) $t = 373.2$ s: 10 roll waves, (f) $t = 510.6$ s: the start of the 6-wave state, and (g) $t = 40\,000$ s: the same state at a much later time, when the 6 roll waves have become identical.

IV. TWO COMPETING MECHANISMS

The N-wave state starts immediately after a merging event takes place in the $(N + 1)$-wave state and ceases to exist after a time τ_N when a new merging occurs. At this point, the $(N - 1)$-wave state begins, and so on and so forth until finally the arrested state with $N = N_{\text{arr}}$ waves is reached.

There are two competing mechanisms which together set the lifetime τ_N of the N-wave state: On the one hand, large roll waves travel faster than small ones, which leads to merging. On the other hand, the waves (large and small) all tend to adjust their amplitude to a preferential height h_{eq}, which means that the velocity differences between them diminish in time, thereby decelerating the merging.

This article is copyrighted as indicated in the article. Reuse of AIP content is subject to the terms at: http://scitation.aip.org/termsconditions. Downloaded to IP: 150.140.170.210 On: Mon, 29 Dec 2014 14:07:55

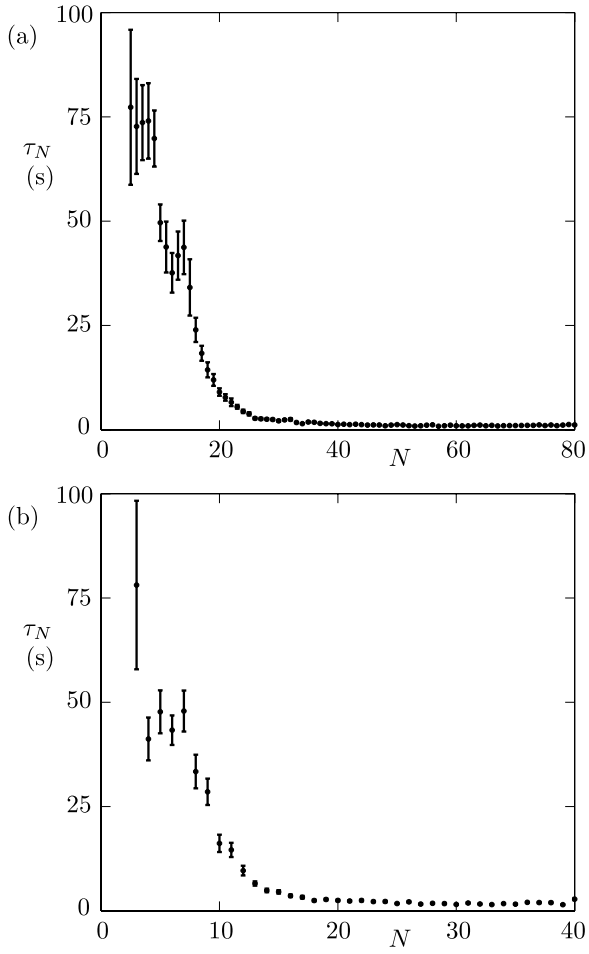

FIG. 7. The numerically observed lifetimes τ_N (solid dots), averaged over the number of times each N-wave state is observed as a transient stage: (a) for a chute of length $L = 50$ m, where the coarsening is never observed to reach lower values than $N = 4$ (and hence there are no finite values of τ_N for $N \leq 4$) and (b) for a chute of length $L = 25$ m, where the minimal observed number of waves is $N = 2$ (and hence no finite lifetimes are found for $N \leq 2$). The error bars represent the standard error of each lifetime τ_N.

A. First mechanism: Larger waves travel faster

Regarding the first mechanism, we will derive a quantitative relation between the wave speed u_w and the height of the peaks by considering each roll wave as a discontinuous shock. That is, we consider the zero viscosity limit $\nu \to 0$, which is a sensible approximation, given the very steep slope at the shock front (see Fig. 8). The Rankine-Hugoniot conditions for the mass and momentum conservation across the shock [cf. Eqs. (2) and (3)] are then given by[21]

$$[h(\bar{u} - u_w)]_-^+ = 0 \tag{15}$$

and

$$\left[h\bar{u}(\bar{u} - u_w) + \tfrac{1}{2}gh^2 \cos\zeta\right]_-^+ = 0, \tag{16}$$

respectively, where the jump bracket $[f]_-^+ = f_+ - f_-$ denotes the difference in value of the enclosed quantity f on the forward "+" and rearward "−" sides of the jump, which travels downslope at the constant speed u_w of the traveling wave. The first jump condition (15) may be rearranged to give the rearward side depth-averaged velocity as

$$\bar{u}_- = u_w + \frac{h_+}{h_-}(\bar{u}_+ - u_w). \tag{17}$$

This article is copyrighted as indicated in the article. Reuse of AIP content is subject to the terms at: http://scitation.aip.org/termsconditions. Downloaded to IP: 150.140.170.210 On: Mon, 29 Dec 2014 14:07:55

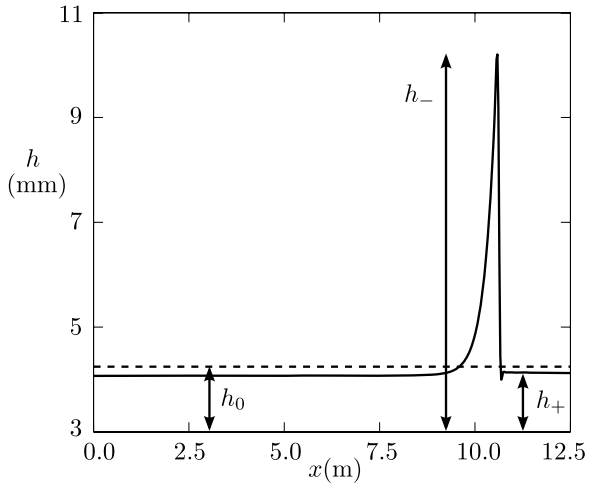

FIG. 8. The flow thickness h_+ on the forward side of the wave crest, here considered as an inviscid shock, is observed to be approximately equal to the uniform flow thickness h_0 (dashed line). The depicted wave, with a height on the rearward side of the jump of $h_- = 10.2$ mm, is one of the two waves which remain in an arrested state after developing from a randomly perturbed uniform flow on a periodic chute of length $L = 25$ m; the snapshot is taken at a simulation time of $t = 465$ s.

Replacing $\bar{u}_-$ with (17) in the second jump condition (16) and canceling common factors $h_+ - h_-$, which is permitted since $h_+ \neq h_-$ (see Fig. 8), yields a quadratic equation for the wave speed u_w

$$h_+ u_w^2 - 2h_+\bar{u}_+ u_w + h_+\bar{u}_+^2 - \tfrac{1}{2}g\cos\zeta(h_+ + h_-)h_- = 0, \tag{18}$$

which has two roots

$$u_w(h_-) = \bar{u}_+ \pm \sqrt{\frac{1}{2}g\cos\zeta\big[1 + (h_-/h_+)\big]h_-}\,. \tag{19}$$

Our numerical observations show that the flow thickness on the forward side of the jump is only slightly below the uniform flow thickness h_0 (see Fig. 8), since the accumulated mass in the wave peak is taken evenly from across the wavelength. It is thus a reasonable approximation to set $h_+ = h_0$ and $\bar{u}_+ = \bar{u}_0$. Identifying the thickness on the rearward side of the shock with the peak height, $h_- = h_w$, Eq. (19) then takes the form

$$u_w(h_w) = \bar{u}_0 + \sqrt{\frac{1}{2}g\cos\zeta\big[1 + (h_w/h_0)\big]h_w}\,, \tag{20}$$

where we have kept only the root with the plus sign, since $u_w > \bar{u}_0$ for a roll wave. This formula for the wave speed is depicted in Fig. 9 (solid line) together with numerical measurements on chutes of varying length. The agreement is seen to be very good, justifying the various assumptions we made in the derivation of Eq. (20).

The analysis can be simplified further by linearizing the expression (20) about $h_w = h_0$. Up to first order in $(h_w - h_0)$ we then obtain

$$\begin{aligned} u_w(h_w) &= \bar{u}_0 + \sqrt{g h_0 \cos\zeta} + K(h_w - h_0) + \cdots \\ &= u_g + K(h_w - h_0) + \cdots, \end{aligned} \tag{21}$$

where the dots indicate the neglected higher order terms in the small variable $(h_w - h_0)$. The velocity $u_g = \bar{u}_0 + \sqrt{g h_0 \cos\zeta}$ may be recognized as the speed of gravity waves in the uniform flow, and the constant K is given by

$$K = \tfrac{3}{4}\sqrt{g\cos\zeta/h_0}\,. \tag{22}$$

Figure 9 shows that the linear approximation (21) is in good agreement with both the full expression (20) and numerical observations of the wave speed u_w. Thus, we have established the relation between the speed of a granular roll wave and its peak height.

This article is copyrighted as indicated in the article. Reuse of AIP content is subject to the terms at: http://scitation.aip.org/termsconditions. Downloaded to IP: 150.140.170.210 On: Mon, 29 Dec 2014 14:07:55

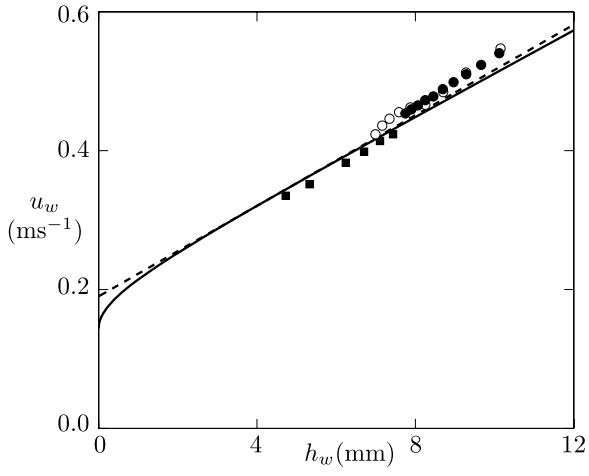

FIG. 9. The speed of the roll wave u_w as function of its peak height h_w. The solid dots are numerical data from a 50 m chute, the open dots correspond to a chute of 25 m, while the solid squares are collected from various short chutes with $0.3 < L < 3.2$ m. The solid curve is the theoretical prediction Eq. (20) from the inviscid shock wave approximation; the straight dashed line is a linearization of the latter about $h_w = h_0$, given by Eq. (21).

B. Upper bound on the wave peak height

In the same inviscid limit ($\nu \to 0$), it can be shown that the peak height of the roll waves must always remain smaller than a certain upper bound. This is of crucial importance in the context of the present paper, since the arrested coarsening is a direct consequence of it: in a long chute, the granular material cannot accumulate in a single roll wave (because the peak height of this wave would violate the upper bound) and therefore the mass must necessarily be distributed over two or more roll waves. Our derivation of the upper bound starts from the observation that the roll wave is a traveling wave solution of Eqs. (2)-(3), which we exploit (in the spirit of Dressler[6]) to gather information on the characteristic shape of the wave.

A traveling wave solution to the equations of motion (2)-(3), propagating in the positive x direction at speed u_w, is most conveniently described in the variables of the co-moving frame

$$\xi = x - u_w t, \quad \tau = t. \tag{23}$$

Thus, we follow the wave in the coordinate system (ξ, τ) that remains at all times centered at the wavefront; in this frame $h = h(\xi, \tau)$ and $\bar{u} = \bar{u}(\xi, \tau)$. As a matter of fact, for a traveling wave in the steady state we demand $\partial h/\partial \tau = 0$ and $\partial \bar{u}/\partial \tau = 0$. The continuity and momentum equations (2)-(3) then reduce to

$$\frac{\mathrm{d}}{\mathrm{d}\xi}\left((\bar{u} - u_w)h\right) = 0, \tag{24}$$

$$(\bar{u} - u_w)h\frac{\mathrm{d}\bar{u}}{\mathrm{d}\xi} = hg\sin\zeta - \mu hg\cos\zeta - hg\cos\zeta\frac{\mathrm{d}h}{\mathrm{d}\xi}, \tag{25}$$

where in the latter equation we have taken the inviscid limit $\nu \to 0$, and divided throughout by h. Note that, as a consequence of the fact that we now focus on steady traveling wave solutions, all partial derivatives of the original equations have been replaced by the straight derivative $d/d\xi$ (since ξ is the only remaining variable): the Eqs. (24)-(25) are *ordinary* differential equations (ODEs).

The continuity equation (24) tells us that the discharge rate of granular material (or volumetric flux per unit width) with respect to the co-moving frame of reference is constant

$$(\bar{u} - u_w)h = M. \tag{26}$$

The value of the constant M can be determined by substituting the values of h and $\bar{u}$ at any point along the wave. Taking the point where $h = h_+$ and $\bar{u} = \bar{u}_+$ (Fig. 8) we see that $M = (\bar{u}_+ - u_w)h_+$

This article is copyrighted as indicated in the article. Reuse of AIP content is subject to the terms at: http://scitation.aip.org/termsconditions. Downloaded to IP: 150.140.170.210 On: Mon, 29 Dec 2014 14:07:55

is in fact negative, because u_w is always larger than any other velocity by the definition of the roll wave.

For waves of a relatively long wavelength (of the order of 1 m and greater, as in Fig. 8), we observe that the peak of the roll wave is followed by a long tail of practically uniform thickness. The flow thickness in this whole region is indistinguishable from $h = h_+$. The corresponding velocity $\bar{u}_+$ may thus be identified as the velocity of a flow of uniform thickness h_+, suggesting that we may use Eq. (8) to write

$$(\bar{u} - u_w)h = M = (Bh_+^{3/2} - u_w)h_+, \tag{27}$$

where the constant $B = \beta\sqrt{g\cos\zeta}/(\mathscr{L}\gamma)$ has been introduced in Sec. II. Rearranging Eq. (27) gives the depth-averaged velocity $\bar{u}$ everywhere as a function of flow thickness h

$$\bar{u} = u_w + \frac{h_+}{h}\left(Bh_+^{3/2} - u_w\right), \tag{28}$$

which upon substitution into the momentum equation (25) gives a first order ODE for the flow thickness,

$$\frac{\mathrm{d}h}{\mathrm{d}\xi} = \frac{h^3 g(\sin\zeta - \mu\cos\zeta)}{h^3 g\cos\zeta - h_+^2\left(Bh_+^{3/2} - u_w\right)^2}. \tag{29}$$

Somewhere along the roll wave profile, at the rear slope of the wave, the flow thickness attains the critical value $h = h_{\mathrm{crit}}$, where the denominator in the above expression is zero. At this point, the Froude number measured in the co-moving frame $\left(\mathrm{Fr}_{\mathrm{co}} = |\bar{u} - u_w|/\sqrt{gh\cos\zeta}\right)$ passes through 1, separating the wave in two fundamentally different sections: one section where the height exceeds h_{crit} and hence $\mathrm{Fr}_{\mathrm{co}} < 1$ (subcritical flow), and one section where $h < h_{\mathrm{crit}}$ and hence $\mathrm{Fr}_{\mathrm{co}} > 1$ (supercritical flow). Note that in the co-moving frame we are considering here, owing to the fact that the flux M is negative, the grains move to the left, from the shock front to the tail.

When the denominator in (29) becomes zero, it is necessary to also set the numerator to zero, in order to prevent the gradient $\mathrm{d}h/\mathrm{d}\xi$ from becoming infinite.[6] The numerator is zero for $\tan\zeta = \mu$. Now, the friction coefficient μ defined by Eq. (4) can be expressed in terms of h only by using Eq. (28)

$$\mu = \mu(h) = \mu_1 + \frac{\mu_2 - \mu_1}{1 + \frac{\beta h^{5/2}\sqrt{g\cos\zeta}}{\mathscr{L}\left[u_w(h - h_+) + Bh_+^{5/2}\right]}} \tag{30}$$

and with this, the condition $\tan\zeta = \mu(h)$ at the critical point takes the following form:

$$Bh^{5/2} - u_w(h - h_+) - Bh_+^{5/2} = 0, \tag{31}$$

where we have made use of the definitions of the parameters γ [see Eq. (7)] and B [see below Eq. (27)]. Rearranging for the wave speed we obtain

$$u_w = \frac{B\left(h^{5/2} - h_+^{5/2}\right)}{h - h_+}. \tag{32}$$

Similarly, setting the denominator of (29) equal to zero

$$h^3 g\cos\zeta - h_+^2\left(Bh_+^{3/2} - u_w\right)^2 = 0 \tag{33}$$

and solving for u_w gives (we keep only the negative square root because only this corresponds to an admissible wave velocity $u_w > \bar{u}_+$)

$$u_w = Bh_+^{3/2} + \frac{h^{3/2}\sqrt{g\cos\zeta}}{h_+}. \tag{34}$$

Note that this wave speed holds for the entire roll wave (not only for the points featuring in the derivation of the above expression where $h = h_+$ or $h = h_{\mathrm{crit}}$) since the ripened wave moves steadily forward, as a whole, without change of shape.

This article is copyrighted as indicated in the article. Reuse of AIP content is subject to the terms at: http://scitation.aip.org/termsconditions. Downloaded to IP: 150.140.170.210 On: Mon, 29 Dec 2014 14:07:55

Combining (32) and (34), and excluding the solution $h = 0$ (since h_{crit} must obviously be larger than zero), after some algebra yields

$$\left(Bh_+ - \sqrt{g\cos\zeta}\right)h^{3/2} + h_+\sqrt{g\cos\zeta}\,h^{1/2} - Bh_+^{5/2} = 0, \tag{35}$$

which is satisfied at the critical thickness $h = h_{\text{crit}}$ where both the numerator and denominator of Eq. (29) are zero. It is also trivially satisfied for the uniform thickness $h = h_+$ in the tail of the roll wave, but this is not the solution we are looking for here.

The critical thickness $h_{\text{crit}}(h_+)$ which follows from Eq. (35) is an increasing function of h_+. Consequently, it attains its maximum value when h_+ is as close as possible to its upper bound h_0. The peak mass is then the accumulation of an extremely thin layer of grains taken away from the uniform flow thickness h_0; the corresponding domain length must obviously be quite long. The absolute, never attainable upper bound for the critical thickness $\left(\text{denoted by } h_{\text{crit}}^{\max}\right)$ is obtained by setting $h_+ = h_0$ and in our system turns out to be equal to $h_{\text{crit}}^{\max} = 8.9$ mm.

The associated upper bound to the wave speed is found by substituting this critical thickness $h_{\text{crit}}^{\max}$ into either (32) or (34), yielding $u_w^{\max} = 0.7$ m/s. This in turn sets the upper bound for the peak height of the roll waves, which we will denote by $h_w^{\max}$. Substituting the wave speed $u_w^{\max}$ into our formula for $u_w(h_w)$, Eq. (20), and solving for the peak height, we finally obtain

$$h_w^{\max} = \frac{h_0}{2}\left(-1 + \sqrt{1 + \frac{\left(u_w^{\max} - Bh_0^{3/2}\right)^2}{2gh_0\cos\zeta}}\right), \tag{36}$$

which for the parameter values in our system gives $h_w^{\max} = 16.2$ mm.

The above result is an absolute upper bound on the peak height of a traveling roll wave solution to the inviscid governing equations. It is larger than any of the roll waves observed in our numerical simulations (the largest one of which had a peak height $h_w = 10.4$ mm) for several reasons: (i) the effect of the viscous-like term in the full system of equations (2)-(3) will round off the peaks, (ii) a finite layer of granular matter must be taken away from the uniform flow thickness (to construct the wave peak) which means that the actual value of h_{crit} will in practice always be smaller than $h_{\text{crit}}^{\max}$ and this in turn leads to a smaller peak height, and (iii) the finite resolution of our simulations slightly underestimates the actual peak heights. We have performed several sample simulations with a higher resolution and these yield roll waves that have a somewhat larger peak height than those with the standard resolution.

The existence of a maximum peak height is an important result: it means that the waves cannot grow indefinitely. The fact that the coarsening process in long chutes is arrested in a state with more than 1 wave is an immediate consequence of this.

To close this section, we note that the above analysis involving the critical thickness h_{crit} is not restricted to the absolute maximum found by setting $h_+ = h_0$. Equation (35) holds for all roll waves, not only for the biggest ones. Indeed, inserting the *numerically observed* values of h_+ (instead of h_0) into Eq. (35), we always obtain a critical thickness h_{crit} that yields [via either Eq. (32) or (34)] a corresponding wave speed u_w. From this wave speed one obtains, using Eq. (20), the associated peak height h_w. The resulting pair of h_w and u_w is invariably found to be in very good agreement with Fig. 9 along the entire curve.

C. Second mechanism: Wave height relaxation

As for the second mechanism, the equilibrium wave height h_{eq} gradually grows as the coarsening process proceeds towards smaller values of N, just as one would expect. As a matter of fact, our numerical simulations reveal a universal trend indicating that h_{eq} is an increasing function of the average *separation distance* ($s = L/N$) between successive waves, rather than of N alone. When the equilibrium heights h_{eq} are plotted as a function of s for chutes of different lengths L (as in Fig. 10) all data are seen to collapse onto a single curve

$$h_{\text{eq}}(s) = h_0 + Cs^{\eta}, \tag{37}$$

This article is copyrighted as indicated in the article. Reuse of AIP content is subject to the terms at: http://scitation.aip.org/termsconditions. Downloaded to IP: 150.140.170.210 On: Mon, 29 Dec 2014 14:07:55

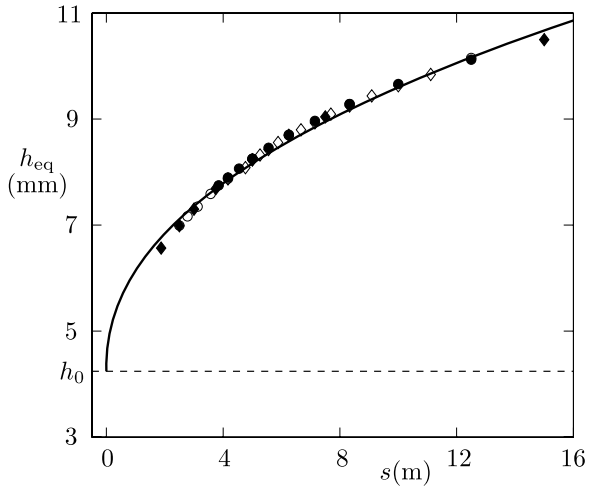

FIG. 10. The equilibrium peak height h_{eq} as a function of the average separation distance between the waves, $s = L/N$. The data from chutes with different domain lengths L are seen to collapse onto a single universal curve; the solid line represents the fit to the data given by Eq. (37). It stops at $s = 15$ m, which is the maximal separation distance (for the parameters used in this paper). The solid diamonds correspond to a domain length $L = 15$ m, the open dots to $L = 25$ m, the solid dots to $L = 50$ m, and the open diamonds to $L = 100$ m. In the limit $s \to 0$, the peak height h_{eq} reduces to the steady uniform flow thickness h_0 (dashed horizontal line): the amplitude of the roll wave ($N = 1$) vanishes, and hence the wave ceases to exist, as the chute length L tends to zero.

where h_0 is the thickness of the unperturbed bed, and C and η are fit parameters. The best fit to our numerical data (given by the solid curve in Fig. 10) was obtained with a prefactor $C = 0.0019$ and exponent $\eta = 0.45$.

The curve stops at $s \approx 15$ m. The measurement at $s = 15$ m in Fig. 10 corresponds to an arrested 1-wave state in a 15 m periodic chute, and this is the largest wavelength we have ever observed. For longer chutes (with a periodic domain length $L > 15$ m), the number of waves in the arrested state is always greater than 1. So when $15\ \text{m} < L < 30$ m the coarsening process will be arrested in a state with at least 2 waves. The 2-wave case (with a separation distance $L/2$ varying between 7.5 m and 15 m) is the most ripened form for this domain length, and in practice the coarsening will be often arrested in a state with several more waves depending on the initial, random perturbations of the uniform flow; note that this agrees precisely with our observations of the arrested states for the 25 m chute of Fig. 7(b). Similarly, for $30\ \text{m} < L < 45$ m, the coarsening will stop in a state with at least 3 waves (with $s = L/3$ varying between 10 m and 15 m) and usually several more. This periodic extension of the basic 15 m domain can be continued indefinitely. For instance, if $45\ \text{m} < L < 60$ m, the arrested state will consist of minimally 4 roll waves (with $s = L/4$ varying between 11.25 m and 15 m), and usually several more, in full agreement with the numerical data for our standard chute with $L = 50$ m.

The existence of a maximal separation distance (15 m for the parameters we are using) tells us that there is a natural length unit in the direction of the flow: increasing the length L of the domain beyond this value is equivalent to periodically extending the unit system. The maximal separation distance, or wavelength, in a chute of any domain length L can be inferred from the curve in Fig. 10. For increasing L, as the examples of the previous paragraph show, the maximal wavelength is selected from an ever-decreasing part of the upper end of this curve. In the limit $L \to \infty$, for the rarely observed arrested state with maximal wavelength (i.e., minimal number of waves), all roll waves will have a separation distance close to 15 m and a peak height of about 10.5 mm. Note that these numbers depend on the parameters in the governing equations and constitutive relations (such as g, γ, and $\mathscr{L}$) and in the concluding section we will briefly discuss how our results can be upscaled to be compatible with real geophysical flows, where granular roll waves are observed to reach amplitudes up to 1 m or more.

This article is copyrighted as indicated in the article. Reuse of AIP content is subject to the terms at: http://scitation.aip.org/termsconditions. Downloaded to IP: 150.140.170.210 On: Mon, 29 Dec 2014 14:07:55

Now let us turn our attention to a typical N-wave state during the coarsening process. During the lifetime of such a state, the roll waves tend to adjust their peak height to the equilibrium value $h_{eq}(s)$, by shedding off or picking up mass. This is illustrated in Fig. 11 for a 4-wave state in a periodic chute of 50 m; for clarity we here show the ripening of a final arrested state, which means that the convergence to $h_{eq}(s)$ is not interrupted by any merging event as it would for an intermediate N-wave state. The peak heights of the four waves are seen to oscillate, as they shed off and pick up material, and collectively converge to the value $h_{eq}(50/4) = 10.1$ mm.

A particularly insightful way to view the relaxation process is presented in Fig. 12(a), which shows the ripening of the roll waves in $(h, \mathrm{d}h/\mathrm{d}\xi)$ phase space (where ξ is the traveling wave coordinate introduced in Subsection IV B). It is seen that the trajectories corresponding to the profiles of the developing roll waves converge towards a stable limit cycle.[14] Waves that are initially too large start in the outer part of the shaded region: they spiral inward to the limit cycle, cross it somewhere along the segment E-F, and then proceed in the inner part of the shaded region until they cross the segment E-F again, and so on. The amplitude of the excursions from the limit cycle decreases gradually until the trajectory becomes indistinguishable from the limit cycle itself. This explains the oscillatory convergence of the peak heights observed in Fig. 11; the peak height $h_{eq}(s)$ corresponds to the point indicated by the letter A in Fig. 12(a), where $h(\xi)$ is maximal (10.1 mm) and $\mathrm{d}h/\mathrm{d}\xi = 0$.

Waves that are initially too small exhibit the same behavior, only now starting out from a position in the inner part of the shaded region. The start of an arrested 2-wave state is shown in Fig. 12(b), where the waves I (initially too small) and II (initially too large) correspond to the boundaries I and II of the shaded area in Fig. 12(a).

The oscillatory convergence to the equilibrium height is only observed when there are at least 2 waves in the system, and is a manifestation of the exchange of mass between the waves (by shedding off material, which is then being picked up by the next). In a situation with only 1 wave, such as may be encountered in a chute with a short domain length, the convergence is monotonous.

The letters B-F indicate five further characteristic points along the wave, and Fig. 12(c) shows the full correspondence between the limit cycle in $(h, \mathrm{d}h/\mathrm{d}\xi)$ phase space and the structure of the ripened roll wave. At point B, the derivative $\mathrm{d}h/\mathrm{d}\xi$ goes through its minimum value, corresponding to the position on the steeply descending wavefront where the profile turns from being convex to concave. Point C is located near the foot of the wavefront, where h passes through the value $h_0 = 4.2$ mm, soon thereafter to be followed by point D where the wave attains its lowest level ($h = 3.95$ mm). The part of the limit cycle between D and E, small as it may be, corresponds to the

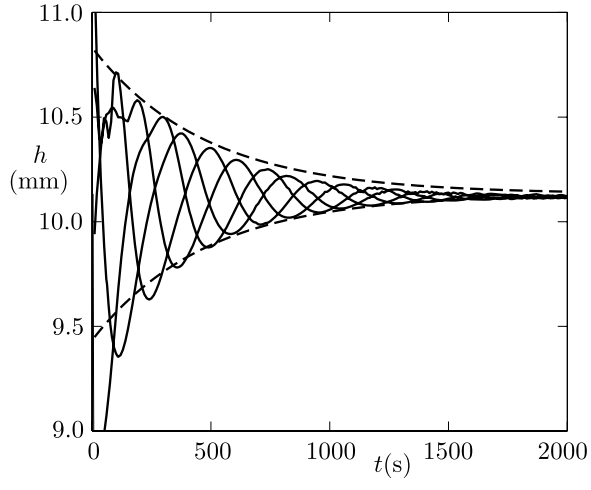

FIG. 11. Relaxation of the peak heights of four roll waves toward the equilibrium value $h_{eq}(50/4) = 10.1$ mm in a chute of length $L = 50$ m. The time $t = 0$ s coincides with the merging event that commences the 4-wave state (which happens to be the state in which the coarsening process is arrested in this particular run). The oscillations correspond to the periodic shedding off and picking up of mass by the waves in their attempt to adjust their heights to $h_{eq}(50/4)$. The dashed envelope curves indicate the exponential decay (and growth) described by Eq. (39), with parameters $\lambda = 0.0021\ \mathrm{s}^{-1}$ and $\alpha = 0.07$.

This article is copyrighted as indicated in the article. Reuse of AIP content is subject to the terms at: http://scitation.aip.org/termsconditions. Downloaded to IP: 150.140.170.210 On: Mon, 29 Dec 2014 14:07:55

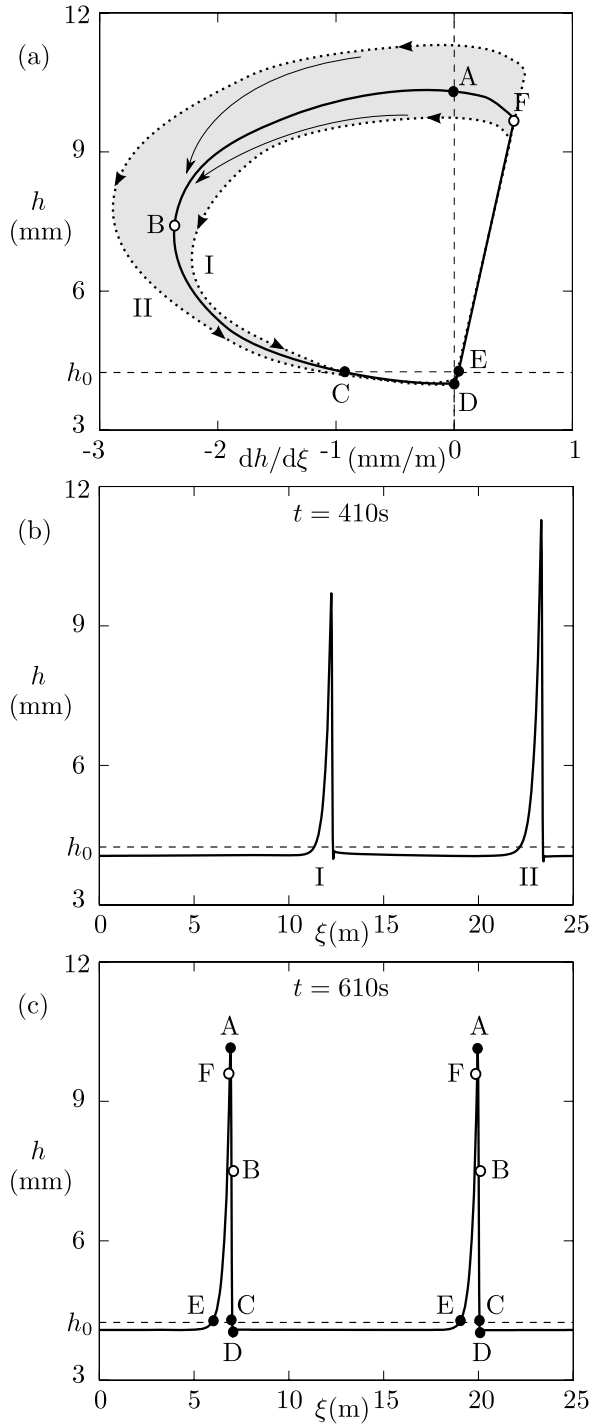

FIG. 12. (a) In (h, dh/dξ) phase space, the ripening of roll waves to their equilibrium shape shows up as a convergence of the waves' phase space trajectories to a stable limit cycle (solid closed curve). (b) The start of the final 2-wave state on a 25 m chute, just after the merger of the large leading wave with a third wave. These waves correspond to the boundaries I and II of the shaded area in the phase space plot (a), and in the course of time they ripen and converge towards the limit cycle, exploring the entire shaded region along the way. (c) Connection between the limit cycle and the profile of the same two roll waves in the long time limit, when they have reached the (arrested) equilibrium state. The points A-F along the roll waves correspond to the same six points on the limit cycle.

This article is copyrighted as indicated in the article. Reuse of AIP content is subject to the terms at: http://scitation.aip.org/termsconditions. Downloaded to IP: 150.140.170.210 On: Mon, 29 Dec 2014 14:07:55

long (practically horizontal) tail of the roll wave. Finally, at point E the height h passes through the value h_0 again and from here rises all the way to points F and A, after which the cycle is repeated.

Point F (where the derivative $\mathrm{d}h/\mathrm{d}\xi$ goes through its maximum value) corresponds to the position on the upward flank of the wave where the profile changes from concave to convex. Interestingly, the segment of the limit cycle between E and F is seen to be practically straight: $h = a + b\mathrm{d}h/\mathrm{d}\xi$, from which it can be inferred that the wave profile from E to F in Fig. 12(c) rises (in good approximation) exponentially, as $h - a \propto \exp(\xi/b)$.

According to standard stability theory, the nearby phase space trajectories will approach the limit cycle in such a way that their distance to the limit cycle decreases exponentially in time, as $\exp(-\lambda t)$, where $-\lambda$ is the Lyapunov exponent. In agreement with this, we find that the peak heights of the waves converge exponentially to the equilibrium value h_{eq} exponentially (with t_N denoting the moment when the N-wave state comes into existence)

$$h_{w,i}(t) - h_{\mathrm{eq}} = \left[h_{w,i}(0) - h_{\mathrm{eq}}\right] e^{-\lambda(t-t_N)}, \tag{38}$$

for all waves $i = 1, 2, .., N$. A similar relaxation phenomenon was observed by Chang *et al.* in a model for roll waves in water.[31] The convergence rate (or negative Lyapunov exponent) λ appears to be fairly independent of N. For sufficiently long chutes, it also does not depend sensitively on the domain length L; from our simulations on the 50 m chute we find $\lambda = 0.0021\ \mathrm{s}^{-1}$ and the same value fits the data from the 25 m chute reasonably well. For significantly shorter chutes, in which the waves are recycled more frequently and therefore interact more strongly, the adjustment to the equilibrium height is somewhat faster, corresponding to a higher value of λ.

For a "typical" wave, whose peak height (according to our simulations) at $t = t_N$ deviates only a few percent from the target value $h_{\mathrm{eq}}(s)$, the above relaxation to the equilibrium height can also be expressed as follows:

$$\left|h_{\mathrm{typ}}(t) - h_{\mathrm{eq}}\right| = \alpha h_{\mathrm{eq}} e^{-\lambda(t-t_N)}, \tag{39}$$

with α (the typical deviation) being of the order of 0.07, i.e., seven percent. This is in fact the value which has been used in Fig. 11 to construct the dashed envelope curves. The parameter α is intrinsically noisy, conveying the memory of the random initial conditions, and in our various numerical runs is found to vary between 0.05 and 0.09 (without any systematic dependence on N or L). Within these bounds we may therefore treat it as a free fit parameter.

Two different time scales can be assigned to the above two competing mechanisms: (i) the target time $t_{\mathrm{target},N}$, being the average distance between two successive waves divided by their typical velocity difference at the start of the N-wave state (which in the absence of the second mechanism would be equal to the catch-up time), and (ii) the relaxation time $t_{\mathrm{relax}} = 1/\lambda = 480$ s associated with the convergence to the preferential peak height. In the early stages of the coarsening process, when the average distance between the waves ($s = L/N$) is small, the time scale $t_{\mathrm{target},N}$ is much smaller than t_{relax} and we observe a number of merging events in rapid succession; the value of N thus quickly decreases. As time goes by, however, the system enters a different regime. When $t_{\mathrm{target},N}$ becomes of the same order of magnitude as t_{relax}, and the influence of the relaxation is increasingly felt, the coarsening process slows down drastically. Some time later, when $t_{\mathrm{target},N}$ significantly exceeds t_{relax}, the waves are given the opportunity to adjust their height to the equilibrium height before any merging event takes place. All the remaining waves in the system then travel with the same speed (because they all have the same height) and the coarsening process comes to a halt. The average distance between the waves in this arrested state, denoted s_{arr}, may be viewed as the natural wavelength of the system, and the physical interpretation of the coarsening process from this perspective is that of an intricate mechanism for spontaneous wavelength selection.

The corresponding value of N, which we call N_{arr}, is derived in Sec. V together with a theoretical expression for the lifetimes τ_N that quantitatively reproduces the simulation results of Sec. III.

This article is copyrighted as indicated in the article. Reuse of AIP content is subject to the terms at: http://scitation.aip.org/termsconditions. Downloaded to IP: 150.140.170.210 On: Mon, 29 Dec 2014 14:07:55

V. DERIVATION OF THE COARSENING LAW

A. Typical lifetime of the *N*-wave state

In the N-wave state, the average distance separating the waves is $s = L/N$. This is the distance the larger wave must gain in order to catch up with the smaller one. The time it takes for this to happen (denoted by $T_{\rm av}$) is determined by the velocity difference between the two waves, δu, as follows:

$$\int_0^{L/N} ds = \int_0^{T_{\rm av}} \delta u \, dt, \tag{40}$$

where the time variable t has been put to zero at the start of the N-wave state. With $\delta u = K\delta h$ by (21) the above equation can also be written as

$$\frac{L}{N} = K \int_0^{T_{\rm av}} \delta h \, dt, \tag{41}$$

where K is the constant given by Eq. (22); its value for the present setup is $K = 32.8\ {\rm s}^{-1}$.

Now we use Eq. (39) to set $\delta h(t) = \alpha h_{\rm eq}(s)\exp(-\lambda t)$ (the typical peak height difference between two neighboring waves in the system). With these substitutions the integral in Eq. (41) can be evaluated directly

$$\begin{aligned}\frac{L}{N} &= \alpha K h_{\rm eq}(s) \int_0^{T_{\rm av}} e^{-\lambda t}\, dt \\ &= \frac{\alpha}{\lambda} K h_{\rm eq}(s) \left(1 - e^{-\lambda T_{\rm av}}\right)\end{aligned} \tag{42}$$

or, equivalently, with $L/N = s$

$$T_{\rm av} = -\frac{1}{\lambda} \ln\left(1 - \frac{\lambda s}{\alpha K h_{\rm eq}(s)}\right). \tag{43}$$

What we have done until now is to evaluate the catch-up time for an average pair of waves, i.e., with average distance between the two waves and average velocity difference. This is evidently *not* the same as the lifetime τ_N, which is the catch-up time for the pair that merges *first* (since this event ends the N-wave state and heralds the beginning of the state with $N-1$ waves). In other words, τ_N is the *minimum* catch-up time from the ensemble of all wave pairs.

Now, as long as N is sufficiently large, it is reasonable to assume that the time $T_{\rm av}$ represents the average over a set of statistically independent catch-up times T_i, $i = 1, 2, .., N$, which may be assumed to follow an exponentially decaying probability distribution $P(T_i) = T_{\rm av}^{-1}\exp(-T_i/T_{\rm av})$. A basic property of the exponential distribution is that the expected minimum value (i.e., the smallest element in a set of N randomly chosen numbers obeying this distribution) decreases with the sample length as $1/N$. That is, the expected minimum T_i-value in the set (alias τ_N) is $T_{\rm av}/N$. So we obtain

$$\tau_N = \frac{T_{\rm av}}{N} = -\frac{1}{\lambda N} \ln\left(1 - \frac{\lambda s}{\alpha K h_{\rm eq}(s)}\right), \tag{44}$$

or equivalently, bringing out the dependence on N and L as explicitly as possible

$$\tau_N = -\frac{1}{\lambda N} \ln\left(1 - \frac{\lambda (L/N)}{\alpha K \left[h_0 + C(L/N)^\eta\right]}\right), \tag{45}$$

where we have rewritten the equilibrium height $h_{\rm eq}(s)$ in the form of Eq. (37) and have replaced s by L/N.

B. The maximal wavelength $s_{\rm arr}$ and the associated minimum number of roll waves

One of the most striking features of the coarsening law derived above is that $T_{\rm av}$ (and hence also τ_N) exhibits asymptotic behavior. That is, its value becomes infinite at a certain wavelength $s = s_{\rm arr}$

This article is copyrighted as indicated in the article. Reuse of AIP content is subject to the terms at: http://scitation.aip.org/termsconditions. Downloaded to IP: 150.140.170.210 On: Mon, 29 Dec 2014 14:07:55

where the argument of the logarithm in Eq. (43) becomes zero

$$s_{\mathrm{arr}} = \frac{\alpha K h_{\mathrm{eq}}(s_{\mathrm{arr}})}{\lambda}. \tag{46}$$

By virtue of Eq. (37) this can also be written as

$$\alpha K C s_{\mathrm{arr}}^{\eta} - \lambda s_{\mathrm{arr}} + \alpha K h_0 = 0, \tag{47}$$

which can readily be solved numerically. The number of waves in the arrested state, $N = N_{\mathrm{arr}}$, is simply given by $N_{\mathrm{arr}} = L/s_{\mathrm{arr}}$.

Note that s_{arr} is fully determined by the various coefficients characterizing the two competing mechanisms (overtaking and relaxation) that between themselves govern the progress of the coarsening. Given the values of the various parameters concerning overtaking ($K = 32.8\ \mathrm{s}^{-1}$), relaxation ($\lambda = 0.0021\ \mathrm{s}^{-1}$, $C = 0.0019\ \mathrm{m}^{1-\eta}$, and $\eta = 0.45$) and the estimated spread of the peak heights ($\alpha = 0.07 \pm 0.02$) we find that the maximal wavelength in the arrested state can assume any value between $s_{\mathrm{arr}} = 6.789$ (for $\alpha = 0.05$) and $s_{\mathrm{arr}} = 14.885$ (for $\alpha = 0.09$). Its value is seen to depend quite sensitively on the fit parameter α. It is an increasing function of the noisy parameter α, which stands to reason, because a larger spread of the peak height enhances the coarsening process, resulting in an arrested state with less roll waves, or equivalently a larger wavelength s_{arr}. For very small spread ($\alpha \to 0$), the value of s_{arr} tends to zero, and consequently the equilibrium height h_{eq} tends to h_0 (as seen in Fig. 10). This implies that the coarsening process will never really get started in this limit, simply because the roll wave formation is suppressed.

The value $s_{\mathrm{arr}} = 14.885$, for the relatively large spread $\alpha = 0.09$, is in good agreement with the record wavelength of 15 m (observed in a 15 m chute). The best correspondence with our numerical data for the chutes of 50 m and 25 m (for which s_{arr} is observed to be $L/N = 50/4 = 25/2 = 12.5$ m) is found by choosing a value close to $\alpha = 0.08$, or to be precise $\alpha = 0.07918$. The associated values of N_{arr} are 4 and 2, respectively.

These values yield the vertical asymptotes in Fig. 13, where we compare the theoretical expression (45) for the lifetime τ_N with the numerically obtained lifetimes both for the 50 m chute (Fig. 13(a)) and the 25 m chute (Fig. 13(b)). Evidently, τ_N diverges at the asymptotic values $N = N_{\mathrm{arr}}$.

The overall agreement between the theoretical prediction for τ_N (solid curve) and the numerical data is seen to be quite satisfactory. Interestingly, the accuracy of the prediction is in general better for relatively large values of N than for small ones.

This is partly due to the poorer statistics of the numerical results at small values of N. Another reason is that the assumption of the statistical independence of the merging events (a central ingredient of our model, lying at the basis of the step in which we took $\tau_N = T_{\mathrm{av}}/N$) becomes increasingly audacious when the number of waves decreases.

Given that the measured lifetimes in Figs. 13(a) and 13(b) follow the trend described by Eq. (45), we can infer a deeper connection between the two plots, namely, that they are rescaled versions of one another, confirming our earlier observation that the coarsening process on both chutes takes place in essentially the same way.

More specifically, according to our theory, the lifetimes τ_N for the 25 m chute are twice as large as τ_{2N} for the 50 m chute. The different spans of the horizontal axes in Figs. 13(a) and 13(b) are chosen such as to allow a direct comparison: the solid curve in Fig. 13(b) lies twice as high as the corresponding curve in Fig. 13(a), and is identical in all other respects. This can be traced back to the fact that Eq. (45) for τ_N is invariant under the joint transformation

$$\begin{aligned} L &\to kL, \\ N &\to kN, \\ \tau_N &\to \frac{1}{k}\tau_N. \end{aligned} \tag{48}$$

That is to say, if the domain length is stretched by a factor k and the number of waves is multiplied by the same factor, then the lifetime of the newly constructed kN-wave state is $1/k$ times that of the N-wave state on the original chute of length L. This factor $1/k$ has to do with the aforementioned property for a sample of statistically independent catch-up times T_i: if the number of elements in

This article is copyrighted as indicated in the article. Reuse of AIP content is subject to the terms at: http://scitation.aip.org/termsconditions. Downloaded to IP: 150.140.170.210 On: Mon, 29 Dec 2014 14:07:55

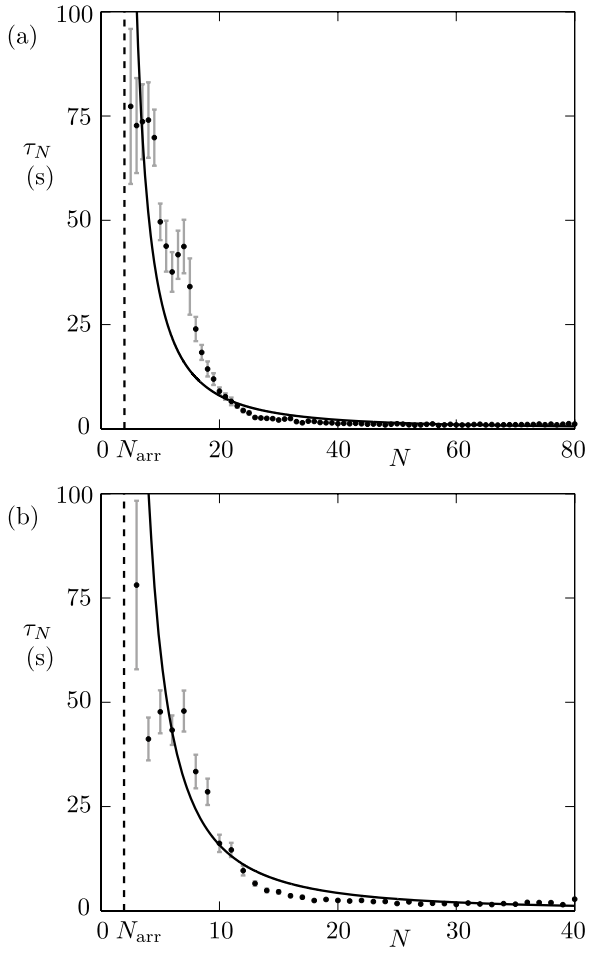

FIG. 13. Comparison of the numerically observed lifetimes τ_N (dots with error bars, cf. Fig. 7) with the theoretical prediction given by Eq. (45) (solid curve) for periodic chutes of length (a) $L = 50$ m and (b) $L = 25$ m. The values of the various coefficients in the theoretical expression are given in the text. The vertical dashed lines denote the asymptotes where the lifetime τ_N diverges: for the 50 m chute this happens at $N_{\rm arr} = 4$ (meaning that the coarsening is arrested, at the very latest, in a 4-wave state) and for the 25 m chute at $N_{\rm arr} = 2$ (corresponding to a 2-wave state).

the sample becomes k times as large, without changing the average value $T_{\rm av}$, the expected value of the smallest element is multiplied by $1/k$. Note that the average value $T_{\rm av}$ [Eq. (43)] remains indeed unchanged owing to the fact that the average separation distance between the waves, $s = L/N$, is an invariant quantity under the transformation (48).

In short, the results for the 50 m chute can be inferred directly from those for the 25 m chute via the above transformation with $k = 2$. One should only keep in mind that this correspondence holds better for large values of N than for small ones, since it hinges again on the statistical independence of the catch-up times. In our system, this independence appears to be well obeyed as long as the average separation distance $s = L/N$ does not exceed a critical value of about $s_* \approx 2.5$ m (corresponding to the state with $N_* = L/s_*$ waves).

As a matter of fact, following this line of thought, the duration t_* of the coarsening process from its beginning until the state with N_* waves, may be anticipated to be the same for any domain length. If the process passes from $N = N_{\rm init}$ to N_* for a chute of domain length L, the corresponding process on a stretched domain of length kL passes through all states from $N = kN_{\rm init}$ to kN_*. The fact that it has to pass through k times as many states is precisely compensated by the fact that these states live shorter by a factor $1/k$. The duration t_* is equal to the sum of all lifetimes from the start of the

This article is copyrighted as indicated in the article. Reuse of AIP content is subject to the terms at: http://scitation.aip.org/termsconditions. Downloaded to IP: 150.140.170.210 On: Mon, 29 Dec 2014 14:07:55

process to the state with kN_* waves

$$t_* = \tau_{(kN_*)} + \tau_{(kN_*+1)} + \cdots + \tau_{(kN_{\text{init}})} = \sum_{kN_*}^{kN_{\text{init}}} \tau_N \approx \int_{kN_*}^{\infty} \tau_N dN, \tag{49}$$

where in the last step we have used that kN_{init} is typically quite large (and that the corresponding lifetime $\tau_{kN_{\text{init}}}$ is vanishingly small). Note that the above integral, thanks to the transformation (48), is independent of the value of k. This makes these early stages of the coarsening process analogous to Christiaan Huygens' classic tautochrone pendulum, the period of which is independent of the amplitude of its oscillations.

VI. CONCLUDING REMARKS

We have studied the coarsening dynamics of roll waves in granular material flowing down a rough inclined channel of length L, with periodic boundary conditions, focusing upon the fact that the coarsening process is arrested before it arrives at the intuitively expected 1-wave state. We have explained this by taking into account two competing mechanisms: (i) the merging of waves, in which larger waves overtake the smaller ones and swallow them, and (ii) the tendency of all waves in the N-wave state to relax toward an equilibrium height (and corresponding equilibrium velocity) that depends on the average separation distance $s = L/N$ between the waves. The interplay between these two rival mechanisms was used to derive the expected lifetime τ_N of the N-wave state, Eq. (45). This predicted lifetime agrees well with numerical observations (see Fig. 13), including the divergence of τ_N at a certain value $N = N_{\text{arr}}$, at which point the coarsening process is arrested. As a matter of fact, we found that the state with N_{arr} waves is attained only when the initial conditions happen to be such that the coarsening process runs its full course, whereas in practice it usually gets stuck in a state with several more waves. In the final state (either with N_{arr} waves or more), all surviving roll waves eventually attain exactly the same height and velocity and chase each other indefinitely around the system. The average distance between them then does not change anymore, and thus the whole coarsening process may be interpreted as a selection mechanism to arrive at the preferential wavelength of the system. The specific wavelength $s_{\text{arr}} = L/N_{\text{arr}}$ (corresponding to the minimal number of waves in the system) defines the upper bound of the average separation distance between the roll waves.

Although all our simulations have been carried out on periodic chutes of finite domain length L, the results can be translated to arbitrarily long chutes by making use of the fact that any chute can be regarded as a repetition of elementary cells of length s_{arr} (which in our system never becomes larger than 15 m). This has to do with the fact that the equilibrium peak height cannot grow beyond a certain threshold value or, equivalently, that the maximum wavelength cannot grow indefinitely (see Fig. 10); whenever a merging event momentarily produces a wave that exceeds these bounds, the mass of this wave has to be re-distributed by shedding off material that is picked up by the waves that follow. In this way, the coarsening process leads to a natural, self-organized length scale in the flow direction.

For instance, the chutes with $L = 50$ m and 25 m can both be regarded as multiple copies of an elementary cell of length 12.5 m. This is clearly illustrated by Fig. 13 where we see that the coarsening is (at the very latest) arrested in a state with 4 and 2 waves, respectively. In the same way, any arbitrarily long chute can be viewed as consisting of repeated copies of an elementary unit cell. The length of the unit cell may vary but (for the parameter values used in the present paper) will never exceed 15 m; the corresponding maximum peak height in the arrested state is 10.4 mm. Even in the limit $L \to \infty$, where the periodic boundary conditions lose their physical meaning and the system becomes equivalent to an unbounded linear chute, one will never observe larger roll waves. We checked this numerically via a simulation on a chute with length $L = 5000$ m (but with all other parameters unaltered) and also here we found that the peak height of a fully developed roll wave never exceeded 10.4 mm.

This article is copyrighted as indicated in the article. Reuse of AIP content is subject to the terms at: http://scitation.aip.org/termsconditions. Downloaded to IP: 150.140.170.210 On: Mon, 29 Dec 2014 14:07:55

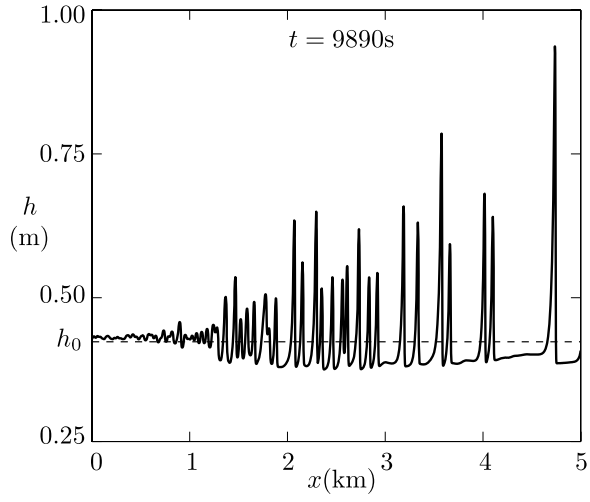

FIG. 14. Roll wave formation on a non-periodic chute of 5 km length, with an inflow thickness ($x = 0$ km) that fluctuates randomly around $h_0 = 0.42$ m. This simulation shows that the height of the roll waves scales roughly linearly with the value of h_0: the value of h_0 is precisely 100 times as large as in all previous simulations, and the peak heights attained at the exit ($x = 5$ km) are of the order of 1 m, i.e., almost 100 times as large as before. The dimensions of this upscaled version of our system (as well as the fact that we do not use periodic boundary conditions) have been chosen such as to enable a comparison with real geophysical flows.

To find higher roll waves, one has to insert more mass in the system. This is easily achieved by upscaling the value of the uniform flow thickness h_0. If one does so, the peak height of the roll waves is found to increase proportionally. This is illustrated in Fig. 14, where we see the results of a 5 km chute without periodic boundary conditions in which h_0 equals 0.42 m, i.e., a hundred times higher than before (which has been done by choosing $\mathcal{L} = 0.1$ m without changing any other parameters except for the automatic change in ν, which is related to $\mathcal{L}$). The roll waves towards the end of the chute are seen to reach heights in the order of 1 m, i.e., almost a hundred times as large as before (and they reach velocities of the order of 5 m/s). This roughly linear scaling can be traced back to the fact that the governing equations (2)-(3) are approximately linear in h, i.e., if $h(x,t)$ is a solution then the upscaled version $Ah(x,t)$ may be expected to be an approximate solution as well. In fact, the continuity equation (2) is exactly linear with respect to h, whereas the momentum balance (3) is linear in h apart from the weak h-dependence in the friction coefficient μ and the nonlinear way in which h appears in the last two terms on the right hand side, representing the depth-averaged pressure gradient and the diffusive term. These departures from linearity will give corrections to the linear scaling but apparently do not affect the general trend too much.

The peak heights and velocities in this upscaled, non-periodic version of our system compare well to granular roll waves observed in real geophysical flows, such as in the Jiang-Jia ravine in China or the Moscardo torrent in the Italian Alps.[32–34]

ACKNOWLEDGMENTS

We wish to thank George Petekidis for insightful comments during a presentation of an early version of this work. D.R. and K.vd.W. are grateful to the School of Mathematics of the University of Manchester, where a substantial portion of the research was performed, for its kind hospitality and financial support under the Grant No. EPSRC EP/I01912X/1 "MAPLE: MAthematics PLatform Engagement activity." They also acknowledge the embedding of this work in the research project "COVISCO," via which this research has been co-financed by the European Union (European Social Fund) and Greek national funds through the Operational Program "Education and Lifelong Learning" of the National Strategic Reference Framework-Research Funding Program THALES: Investing in knowledge society through the European Social Fund (Grant No. MIS 380238). ANE and JMNTG acknowledge support from NERC Grant No. NE/E003206/1 "Segregation and levee

This article is copyrighted as indicated in the article. Reuse of AIP content is subject to the terms at: http://scitation.aip.org/termsconditions. Downloaded to IP: 150.140.170.210 On: Mon, 29 Dec 2014 14:07:55

formation in geophysical mass flows and their feedback on runout distance" as well as EPSRC Grant Nos. EP/I019189/1 "Critical Phenomena and Collective Behaviour of Multi-Particle Complex Systems" and EP/K00428X/1 "Manchester Image Reconstruction and ANalysis" (MIRAN). ANE also acknowledges support from NERC Doctoral training Grant No. NE/G523747/11, as well as travel funding from the EPSRC DTA and the Margaret Elizabeth Lee Fellowship.

[1] F. V. de Blasio, *Introduction to the Physics of Landslides* (Springer, Dordrecht, 2011).
[2] B. Schonfeld, "Roll waves in granular flows and debris flows," Ph.D. thesis (McGill University, Montreal, Canada, 1996).
[3] V. Cornish, *Waves of the Sea and Other Water Waves* (T. Fischer Unwin, London, 1910).
[4] V. Cornish, *Ocean Waves and Kindred Geophysical Phenomena* (Cambridge University Press, 1934).
[5] P. L. Kapitza and S. P. Kapitza, "Wave flow of thin layers of a viscous fluid, III: Eperimental study of undulatory flow conditions ," Zh. Eksperim. i Teor. Fiz. **19**, 105 (1949) [English translation edited by D. ter Haar, *Collected Papers of P. L. Kapitza, Volume II, 1938-1964* (Pergamon Press, Oxford, 1965), pp. 690-709].
[6] R. F. Dressler, "Mathematical solution of problem of roll waves in inclined open channels," Commun. Pure Appl. Math. **2**, 149-194 (1949).
[7] G. B. Whitham, *Linear and Nonlinear Waves* (John Wiley and Sons, New York, 1974). Roll waves are discussed in Sec. 3.2 as a special case of flood waves, pp. 80-91.
[8] L. Debnath, *Nonlinear Partial Differential Equations for Scientists and Engineers*, 2nd ed. (Birkhäuser, Boston, 2005), Roll waves and their stability analysis are treated in Section 6.7, see pp. 302-307.
[9] H.-C. Chang, E. A. Demekhin, E. N. Kalaidin, and Y. Ye, "Coarsening dynamics of falling-film solitary waves," Phys. Rev. E **54**, 1467 (1996).
[10] N. J. Balmforth and S. Mandre, "Dynamics of roll waves," J. Fluid Mech. **514**, 1-33 (2004).
[11] A. Daerr and S. Douady, "Two types of avalanche behaviour in granular media," Nature **399**, 241-243 (1999).
[12] A. J. Holyoake and J. N. McElwaine, "High-speed granular chute flows," J. Fluid Mech. **710**, 35-71 (2012).
[13] S. B. Savage and K. Hutter, "The motion of a finite mass of granular material down a rough incline," J. Fluid Mech. **199**, 177-215 (1989).
[14] J. M. N. T. Gray and A. N. Edwards, "A depth-averaged $\mu(I)$-rheology for shallow granular free-surface flows," J. Fluid Mech. **755**, 503-534 (2014).
[15] P. Jop, Y. Forterre, and O. Pouliquen, "A constitutive relation for dense granular flows," Nature **44**, 727-730 (2006).
[16] O. Pouliquen and Y. Forterre, "Friction law for dense granular flows: Application to the motion of a mass down a rough inclined plane," J. Fluid Mech. **453**, 133-151 (2002).
[17] O. Pouliquen, "Scaling laws in granular flows down rough inclined planes," Phys. Fluids **11**(3), 542-548 (1999).
[18] Y. Forterre and O. Pouliquen, "Flows of dense granular media," Annu. Rev. Fluid Mech. **40**, 1-24 (2008).
[19] J. M. N. T. Gray and C. Ancey, "Segregation, recirculation and deposition of coarse particles near two-dimensional avalanche fronts," J. Fluid Mech. **629**, 387-423 (2009).
[20] A. N. Edwards and J. M. N. T. Gray, "Erosion-depostion waves in shallow granular free-surface flows," J. Fluid Mech. **762**, 35-67 (2015).
[21] J. M. N. T. Gray and X. Cui, "Weak, strong and detached oblique shocks in gravity driven granular free-surface flows," J. Fluid Mech. **579**, 113-136 (2007).
[22] C. G. Johnson and J. M. N. T. Gray, "Granular jets and hydraulic jumps on an inclined plane," J. Fluid Mech. **675**, 87-116 (2011).
[23] X. Cui and J. M. N. T. Gray, "Gravity-driven granular free-surface flow around a circular cylinder," J. Fluid Mech. **720**, 314-337 (2013).
[24] Y. Forterre and O. Pouliquen, "Long-surface-wave instability dense granular flows," J. Fluid Mech. **486**, 21-50 (2003).
[25] B. Scheid, C. Ruyer-Quil, and P. Manneville, "Wave patterns in film flows: Modelling and three-dimensional waves," J. Fluid Mech. **562**, 183-222 (2006).
[26] A. Daerr, "Dynamical equilibrium of avalanches on a rough plane," Phys. Fluids **13**, 2115-2124 (2001).
[27] T. Börzsönyi, T. C. Halsey, and R. E. Ecke, "Two scenarios for avalanche dynamics in inclined granular layers," Phys. Rev. Lett. **94**, 208001 (2005).
[28] T. Börzsönyi, T. C. Halsey, and R. E. Ecke, "Avalanche dynamics on a rough inclined plane," Phys. Rev. E **78**, 011306 (2008).
[29] D. Takagi, J. N. McElwaine, and H. H. Huppert, "Shallow granular flows," Phys. Rev. E **88**, 031306 (2011).
[30] A. Kurganov and E. Tadmor, "New high-resolution central schemes for nonlinear conservation laws and convection-diffusion equations," J. Comput. Phys. **160**, 241-282 (2000).
[31] H.-C. Chang, E. A. Demekhin, and E. N. Kalaidin, "Coherent structures, self-similarity, and universal roll waves coarsening dynamics," Phys. Fluids **12**(9), 2268-2278 (2000).
[32] Li Jan, Yuan Jianmo, Bi Cheng, and Luo Defu, "The main features of the mud flow in Jiang-Jia ravine," Zeit. Geomorph. **27**, 325-341 (1983).
[33] L. Marchi, M. Arattano, and A. M. Deganutti, "Ten years of debris-flow monitoring in the Moscardo torrent, Italian Alps," Geomorphology **46**, 1-17 (2002).
[34] B. Zanuttigh and A. Lamberti, "Instability and surge development in debris flows," Rev. Geophys. **45**, RG3006, doi: 10.1029/2005RG000175 (2007).

This article is copyrighted as indicated in the article. Reuse of AIP content is subject to the terms at: http://scitation.aip.org/termsconditions. Downloaded to IP: 150.140.170.210 On: Mon, 29 Dec 2014 14:07:55